

RESEARCH

Open Access



# Proximity proteomics of C9orf72 dipeptide repeat proteins identifies molecular chaperones as modifiers of poly-GA aggregation

Feilin Liu<sup>1,2†</sup>, Dmytro Morderer<sup>1†</sup>, Melissa C. Wren<sup>1</sup>, Sara A. Vettleson-Trutza<sup>1</sup>, Yanzhe Wang<sup>1,3</sup>, Benjamin E. Rabichow<sup>1</sup>, Michelle R. Salemi<sup>4</sup>, Brett S. Phinney<sup>4</sup>, Björn Oskarsson<sup>5</sup>, Dennis W. Dickson<sup>1</sup> and Wilfried Rossoll<sup>1\*</sup> 

## Abstract

The most common inherited cause of two genetically and clinico-pathologically overlapping neurodegenerative diseases, amyotrophic lateral sclerosis (ALS) and frontotemporal dementia (FTD), is the presence of expanded GGG GCC intronic hexanucleotide repeats in the *C9orf72* gene. Aside from haploinsufficiency and toxic RNA foci, another non-exclusive disease mechanism is the non-canonical translation of the repeat RNA into five different dipeptide repeat proteins (DPRs), which form neuronal inclusions in affected patient brains. While evidence from cellular and animal models supports a toxic gain-of-function of pathologic poly-GA, poly-GR, and poly-PR aggregates in promoting deposition of TDP-43 pathology and neurodegeneration in affected brain areas, the relative contribution of DPRs to the disease process in c9FTD/ALS patients remains unclear. Here we have used the proximity-dependent biotin identification (BioID) proximity proteomics approach to investigate the formation and collective composition of DPR aggregates using cellular models. While interactomes of arginine rich poly-GR and poly-PR aggregates overlapped and were enriched for nucleolar and ribosomal proteins, poly-GA aggregates demonstrated a distinct association with proteasomal components, molecular chaperones (HSPA1A/HSP70, HSPA8/HSC70, VCP/p97), co-chaperones (BAG3, DNAJA1A) and other factors that regulate protein folding and degradation (SQSTM1/p62, CALR, CHIP/STUB1). Experiments in cellular models of poly-GA pathology show that molecular chaperones and co-chaperones are sequestered to the periphery of dense cytoplasmic aggregates, causing depletion from their typical cellular localization. Their involvement in the pathologic process is confirmed in autopsy brain tissue, where HSPA8, BAG3, VCP, and its adapter protein UBXLN6 show a close association with poly-GA aggregates in the frontal cortex, temporal cortex, and hippocampus of c9FTLD and c9ALS cases. The association of heat shock proteins and co-chaperones with poly-GA led us to investigate their potential role in reducing its aggregation. We identified HSP40 co-chaperones of the DNAJB family as potent modifiers that increased the solubility of poly-GA, highlighting a possible novel therapeutic avenue and a central role of molecular chaperones in the pathogenesis of human *C9orf72*-linked diseases.

**Keywords:** C9orf72, Poly-GA, Proximity proteomics, Heat shock proteins

## Introduction

Amyotrophic Lateral Sclerosis (ALS) and frontotemporal dementia (FTD) are progressive neurodegenerative diseases with overlapping clinical, genetic, and neuropathological features that represent the extreme ends of a common FTD/ALS disease spectrum with likely shared

\*Correspondence: rossoll.wilfried@mayo.edu

<sup>†</sup>Feilin Liu and Dmytro Morderer contributed equally to this work and are co-first authors.

<sup>1</sup> Department of Neuroscience, Mayo Clinic, Jacksonville, FL, USA  
Full list of author information is available at the end of the article



pathomechanisms [53, 70, 91]. The most common genetic cause of familial ALS and FTD is a GGGGCC hexanucleotide repeat expansion (HRE) in intron 1 of the *C9orf72* gene locus [18, 77]. Work from several labs across various model organisms have identified three different but non-exclusive disease mechanisms that may contribute to the pathophysiology in human patients [24]. First, HREs may reduce the expression of the *C9orf72* protein, a guanine nucleotide exchange factor (GEF), which plays a role in autophagy [48]. Second, both the sense and antisense sequence forms RNA foci in patients and disease models that sequester cellular proteins, causing nucleocytoplasmic transport defects [16, 62]. Third, repeat RNA can be translated into all 6 reading frames via repeat associated non-ATG (RAN) translation [106]. The resulting dipeptide repeat (DPR) proteins, poly-GA, -GR, -PR, -GP, and -AP form aggregates that can be detected in the brains of FTD/ALS patients with *C9orf72* repeat expansions (c9FTD/ALS) [3, 58, 66]. Studies in cellular and animal models have found significant toxicity for the positively charged arginine-rich poly-GR and poly-PR proteins, and for the highly insoluble poly-GA aggregates [21, 86]. While poly-GP can serve as a pharmacodynamic biomarker for therapy development [23] and targeting poly-GA was found to be therapeutic in *C9orf72* disease models [103], the pathomechanisms and relative contribution of DPR toxicity to human disease are still unclear. This raises important questions about (1) what proteins are sequestered into DPR aggregates, thereby causing cellular defects, and (2) what molecular pathways can modulate the formation and disassembly of DPR aggregates, as potential novel targets for therapeutic intervention.

Previous DPR interactome studies, based on co-immunoprecipitation and proteomic analysis of soluble DPR proteins, have primarily found an association between arginine-rich poly-GR and poly-PR with ribosomal proteins and RNA-binding proteins with low complexity domains (LCDs) [6, 54, 56, 98]. This suggests impairments in ribosome biogenesis and protein translation, as well as defects in the assembly and function of membraneless organelles such as stress granules and nucleoli [32, 39, 49, 64]. Poly-GA aggregates have been less well biochemically characterized, due to their highly detergent-insoluble nature, yet some studies indicate enrichment with proteasome components and other proteins involved in the ubiquitin proteasome system (UPS) [60], mediating impaired protein degradation and induction of endoplasmic reticulum (ER) stress pathways [102]. Despite these earlier studies, the contribution of poly-GA-induced pathology to the pathogenesis of c9FTD/ALS and the nature of molecular mechanisms and cellular pathways targeting these pathological aggregates for protein degradation remain poorly understood.

In this study, we employed the proximity-dependent biotin identification (BioID) approach that allows for the labeling of proximal proteins in living cells and their purification under harsh denaturing conditions [12, 80], to determine the interactome of detergent-insoluble poly-GR, -PR, and -GA aggregates. While the interactome for the arginine-rich proteins overlapped and contained primarily nucleolar and ribosomal proteins, the highly insoluble poly-GA interactome was distinct and enriched not only for proteasome components as reported previously [26, 60, 101], but we also discovered an association with numerous molecular chaperones and other proteins involved in protein folding and protein degradation pathways. Sequestration of these proteins to poly-GA aggregates in cell culture and human autopsy brain tissue suggests downstream defects in specific protein quality control pathways, which may ultimately contribute to the resulting neurodegeneration observed in disease models and human patients. Poly-GA associated protein candidates were extensively validated in both cell culture experiments and human autopsy brain tissue, showing very similar patterns of association with insoluble poly-GA aggregates. In addition, we established that the expression of specific DNAJB family co-chaperones reduced the formation of poly-GA aggregates, similar to their reported activity towards polyglutamine (poly-Q) and  $\alpha$ -synuclein aggregates, therefore expanding their potential value as therapeutic targets for c9FTD/ALS patients.

## Materials and methods

### Cell culture and plasmid transfections

HEK293T cells (ATCC CRL-3216) were cultured in DMEM (Gibco) supplemented with 10% FBS (GenClone) and 1% Pen Strep (Thermo Fisher Scientific) and grown at 37 °C with 5% CO<sub>2</sub>. Cells were transfected using Lipofectamine LTX reagent (Invitrogen) following the manufacturer's instructions.

### DNA constructs

To generate myc-BioID-DPR<sub>x100</sub> plasmids, sequences encoding poly-GR, -PR, and -GA (with alternating codons to avoid RNA repeats) were cloned into the pcDNA3.1 mycBioID plasmid (Addgene plasmid #35700) [80] by replacing the TDP-CTF BamHI/HindIII fragment in pcDNA3.1 mycBioID TDP-CTF [12]. Resulting plasmids encode myc-BioID-(GGGS)<sub>x3</sub>-DPR<sub>x100</sub> fusion proteins. EGFP and mCherry-tagged DPR<sub>x100</sub> plasmids were generated by replacing the BioID NdeI/BamHI fragment in myc-BioID-(GGGS)<sub>x3</sub>-DPR<sub>x100</sub> with EGFP or mCherry. 2xHA-poly-GA was cloned by replacing the PvuI/BamHI fragment of EGFP in EGFP-poly-GA with a double HA tag

(MGYPYDVPDYAGGYPYDVPDYA). Expression constructs for EGFP-tagged SQSTM1, UBXN6, VCP, and HSPA8 (accession numbers #38277 [35], #86464 [75], # 23971 [55], #19487 [30], respectively), as well as mCherry-Calreticulin-N-16 (#55006) were obtained from Addgene. EGFP-tagged Calreticulin was cloned by replacing mCherry AgeI/NotI fragment in mCherry-Calreticulin-N-16 with EGFP from the pEGFP-N1 vector (Clontech).

#### **BioID labeling, affinity purification, and immunoblotting**

HEK293T cells (ATCC CRL-11268) were transfected with expression plasmids for EGFP, myc-BioID-DPR<sub>x100</sub>, or myc-BioID using the Lipofectamine LTX transfection reagent (Invitrogen). Biotin was added to the medium to a final concentration of 50  $\mu$ M the next day. After 24 h, cells were washed three times with ice-cold PBS and lysed in denaturing urea lysis buffer (8 M urea, 50 mM Tris-HCl pH 7.5) for 20 min at room temperature (RT). Cell lysates were sonicated and centrifuged at 21,000 $\times$ g for 20 min. For the pulldown of biotinylated proteins, Streptavidin Sepharose High Performance beads (GE Healthcare, 17511301) were incubated with the lysate sample with constant rotation overnight at 4 °C. Beads were collected by centrifugation and washed three times with urea lysis buffer and three times with 50 mM ammonium bicarbonate. Samples were divided where 15% were used for immunoblotting and silver staining, while the remaining 85% was incubated with 500 ng of sequencing-grade trypsin (Promega, V5111) in ammonium bicarbonate overnight. Beads were spun down and the supernatant was collected and dried using a SpeedVac for LC-MS/MS (see below).

For immunoblotting, samples in Bolt LDS sample buffer were separated in a Bolt 4–12% Bis-Tris polyacrylamide gradient gel (Invitrogen) and proteins were transferred to nitrocellulose membranes with the iBlot 2 Dry Blotting System (Thermo Fisher Scientific). Membranes were blocked with Intercept Blocking Buffer (LI-COR, 92770001) in phosphate-buffered saline (PBS) for 45 min, followed by incubation with anti- $\beta$ -tubulin primary antibody (1:5000, DHSB, E7) overnight at 4 °C, and Alexa Fluor Plus 800-conjugated secondary antibodies (1:10,000, Invitrogen, A32730) in Intercept Blocking Buffer for 1 h at RT. Biotinylated proteins were probed with IRDye 680RD streptavidin (1:10,000, LI-COR, 92668031) and detected on an Odyssey CLx scanner (LI-COR). For silver staining, protein gels were processed with Pierce Silver Stain Kit (Thermo Fisher Scientific, 24612) according to the manufacturer's instructions.

#### **Liquid chromatography tandem mass spectrometry (LC-MS/MS)**

Peptides were resuspended in 2% acetonitrile, 0.1% trifluoroacetic acid, and directly loaded on a 75  $\mu$ m  $\times$  10 cm, 1.9  $\mu$ m particle size, C18 column (Bruker, Bremen, Germany) with Captive Spray emitter. Peptides were separated using a Bruker Nano-elute nUPLC at 500 nL/min. Solvent A=0.1% formic acid, Solvent B=100% Acetonitrile 0.1% formic acid. Gradient conditions=2%B to 35%B over 25 min using a Bruker timsTOF Pro mass spectrometer. Mass spectrometry data was acquired using the diaPASEF PY9 method [63]. The acquisition scheme used for diaPASEF consisted of four 25  $m/z$  precursor windows per 100 ms TIMS scan. Sixteen TIMS scans, creating 64 total windows, layered the double and triple charged peptides on the  $m/z$  and ion mobility plane. Precursor windows began at 400  $m/z$  and continued to 1200  $m/z$ . The collision energy was ramped linearly as a function of the mobility from 63 eV at 1/K0=1.5 Vs cm<sup>-2</sup> to 17 eV at 1/K0=0.55 Vs cm<sup>-2</sup>. Some of the samples have been run twice as technical replicates.

#### **Proteomic data analysis**

Data-independent acquisition (DIA) data was analyzed with the Spectronaut 14 software package (Biognosys) using the DIA targeted library-based search. Libraries were generated by searching the diaPASEF data using the Spectronaut pulsar search engine with the default settings against Uniprot UP000005640 Human (78,120 entries) supplemented with the myc-BioID protein sequence. DiaPASEF data were matched against the resulting libraries using Spectronaut 14 default settings. Briefly, “trypsin/P specific” was set for the enzyme allowing two missed cleavages, fixed modifications were set to cysteine carbamidomethylation, and variable modification were set to peptide N-terminal acetylation and methionine oxidation. For DIA search identification, PSM and Protein Group decoy false discovery was set at 1%. Summarization of protein intensities and statistical comparison of protein abundances between the studied groups was performed with the MSstats R package (version 4.0.1) [11] using R (version 4.1.1.) and Rstudio (version 1.4.1717). Proteins were considered as specific interactors when: (1) the log<sub>2</sub> fold-changes of protein abundances in the corresponding samples comparing to both myc-BioID and EGFP controls were > 1; (2) the Benjamini–Hochberg adjusted  $p$  values in both comparisons were < 0.05; and (3) there were no more than 50% missing values for the protein in the corresponding bait and myc-BioID control samples. Analysis for the enrichment of Gene Ontology (GO) terms and Kyoto encyclopedia of genes and genomes (KEGG) pathways in the obtained

protein datasets was performed with the g:Profiler web-based tool using “Only annotated genes” as the statistical domain scope and Benjamini–Hochberg  $FDR < 0.05$  as the significance threshold [76]. Plotting was performed using ggplot2 (version 3.3.5) [95], ggfortify (version 0.4.12) [92], ggrepel (version 0.9.1), RColorBrewer (version 1.1–2) and heatmap (version 1.0.12) R packages. Protein interaction networks were imported from the STRING database [90] using the interaction combined cutoff score of 0.7 and visualized using the Cytoscape software platform (version 3.8.2) [87]. Venn diagrams were generated using the BioVenn online tool [34].

### Immunofluorescence, image acquisition, and analysis in cell culture

HEK293T cells were grown on poly-L-lysine-coated coverslips overnight and co-transfected with expression plasmids for EGFP or epitope-tagged protein of interest and mCherry or mCherry-tagged-poly GA. Cells were incubated with primary antibodies including anti-myc tag (1:50, DSHB, 9E10), anti-HA tag (1:1000, BioLegend, 901514), anti-BAG3 (1:200, Proteintech, 10599-1-AP), anti-SQSTM1 (1:500, Abcam, ab91526), anti-UBXN6 (1:100, Proteintech, 14706-1-AP), anti-VCP (1:500, Abcam, ab109240), anti-V5 tag (1:500, Invitrogen, R960-25), overnight at 4 °C. After washing in PBS, the coverslips were incubated with Alexa Fluor 488- or 555-conjugated secondary anti-rabbit or anti-mouse antibodies (1:1000, Invitrogen, A32723, A32727, A32731 or A32732) and, where applicable, with DyLight 650-conjugated neutravidin (1:500, Invitrogen, 84607), for 1 h at RT. Nuclei were counterstained with Hoechst 33342 (1:5000, Thermo Fisher Scientific, 62249) and the coverslips were mounted on glass slides using ProLong Glass Antifade Mountant (Invitrogen, P36980).

For high-resolution imaging, z-series were acquired according to the different experimental designs with an ECLIPSE Ti2 fluorescence microscope (Nikon) equipped with a Spectra X multi-LED light engine (Lumencor), single bandpass filter cubes for DAPI, EGFP/FITC, mCherry, and Cy5/AF647 (Chroma), and a ZYLA 4.2 PLUS sCMOS camera (Andor), using NIS Elements HC V5.30 software (Nikon). Within each experiment, all

groups were imaged with the same acquisition settings. Imaging parameters were set so that the obtained pixel fluorescence intensity was within the dynamic range of the camera to avoid overexposure. Out-of-focus blur was removed from z-series of fluorescence images via three-dimensional (3D) deconvolution with the NIS-Elements Advanced Research (V5.30) deconvolution package.

### Co-immunofluorescence on human post-mortem tissue

All post-mortem cases were provided by the Mayo Clinic Florida Brain Bank. Tissue was obtained from patients who were carriers of the *C9orf72* repeat expansion and had a confirmed neuropathological diagnosis of either ALS or frontotemporal lobar degeneration (FTLD). Information on the post-mortem cases is provided in Table 1. Informed written consent was obtained before brain donation and study entry from all patients or their legal next of kin when required. Biological samples were obtained with Mayo Clinic Institutional Review Board approval. Donated brains were fixed in 10% neutral buffered formalin before blocks were sectioned and embedded in paraffin for their preservation and sectioning. Double immunofluorescence staining was performed on 5 µm formalin fixed paraffin embedded (FFPE) tissue sections obtained from the mid frontal cortex, superior temporal cortex and medial temporal lobe containing anterior hippocampus. In brief, FFPE tissue sections from the respective post-mortem human brain areas were deparaffinized by immersion in several successions of xylene and rehydrated through a series of graded ethanol solutions (100%, 90% and 70% ethanol), before rinsing in dH<sub>2</sub>O and equilibration in Tris-buffered saline (TBS). Antigen retrieval was performed by steaming tissue sections in citrate buffer, pH 6 (Dako Target retrieval solution, S2369) for 30 min. Slides were slowly cooled for 15 min and gently rinsed with dH<sub>2</sub>O for 10 min. Sections were permeabilized with TBS containing 0.3% Triton-X 100 at RT for 15 min, washed three times for 5 min with TBS, and subsequently blocked with serum-free protein block (Dako, X0909) for 1 h at RT. Tissues were immunostained with antibodies against poly-GA (1:1000, EMD Millipore, MABN889) together with anti-SQSTM1 (1:200, Abcam, ab91526), anti-HSPA8/HSC70 (1:200,

**Table 1** Demographical data of human post-mortem cases used for co-immunofluorescence validation

Case ID	Clinical Dx	Pathol. Dx	Age	Sex	Genetics	TDP-43 subtype	Braak stage	Thal phase	Brain weight (g)	Disease duration
C9/ALS #1	ALS	ALS	67	M	C9orf72	B	II	0	1240	6
C9/ALS #2	ALS/MCI	ALS	67	F	C9orf72	B	II	0	1080	3
C9/FTD #1	FTD	FTLD	62	M	C9orf72	B	II	0	1060	4

ALS, amyotrophic lateral sclerosis; MCI, mild cognitive impairment; FTD, frontotemporal dementia; FTLD, frontotemporal lobar degeneration; *C9orf72*, chromosome 9 open reading frame 72; TDP-43, transactive response DNA-binding protein 43; Dx, diagnosis; M, male; F, female

Proteintech, 10654-1-AP), anti-VCP (1:200, Abcam, ab109240), anti-UBXN6 (1:200, Proteintech, 14706-1AP) or anti-BAG3 (1:200, Proteintech 10599-1-AP), which were diluted in antibody diluent (Dako, S0809) for overnight incubation at 4 °C in a humidified chamber. The following day sections were washed in TBS containing 0.05% Tween-20 (TBS-T), three times for 10 min each, and incubated with Alexa Fluor conjugated secondary antibodies (1:500, anti-mouse 488 (A32723) and anti-rabbit 555 (A32732), both from Invitrogen), diluted in antibody diluent (Dako, S0809), for 2 h at RT. Sections were washed with TBS-T, three times for 10 min each, and then incubated with Hoechst 33342 (1:1000, Thermo Fisher Scientific, 62249) for 20 min at RT and washed with TBS (twice, for 10 min). Lastly, tissue sections were stained with 1 × True Black lipofuscin autofluorescence quencher (Biotium, 23007) for 30 s and rinsed with dH<sub>2</sub>O for 5 min. Tissue sections were mounted with glass slides using ProLong Glass Antifade Mountant (Invitrogen, P36980) and imaged on an ECLIPSE Ti2 fluorescence microscope (Nikon) as described above, except out-of-focus blur was removed from z-series of fluorescence images via the Clarify.ai module of the NIS-Elements Advanced Research (V5.30) deconvolution package. Great care was taken in selecting imaging parameters to avoid overexposures. In addition to single optical sections for all channels, z-series are also shown as 3D volume rendered views to demonstrate co-localization within cells in 3D.

#### Filter trap assay (FTA)

Filter trap assays were performed essentially as described [96]. Briefly, HEK293T cells were co-transfected with EGFP-tagged poly-GA and either V5-tagged chaperones or the mCherry control plasmid as described above. After a 24 h period of transfection, cells were lysed on ice in Triton X-100 lysis buffer (1% Triton X-100, 15 mM MgCl<sub>2</sub> in PBS), supplemented with Pierce Protease Inhibitor cocktail (Thermo Fisher Scientific, A32965) and 30 units of DNase I. Equal amounts of lysates were centrifuged at 21,000×g at 4 °C for 30 min and insoluble pellets were resuspended in SDS lysis buffer (2% SDS in 100 mM Tris, pH 7.5) for 2 h at RT. Samples were diluted at 1:5 in SDS lysis buffer and filtered through a cellulose acetate membrane (0.2 μm pore size) using the Bio-Dot SF Microfiltration System (BioRad). The membrane was blocked in Intercept Blocking Buffer for 1 h and the protein bands were detected with antibodies against GFP (1:1000, Takara Bio, 632592), followed by Alexa Fluor Plus 800-conjugated secondary antibody (1:10,000, Invitrogen, A32735), and scanned on an Odyssey CLx imaging system (LI-COR).

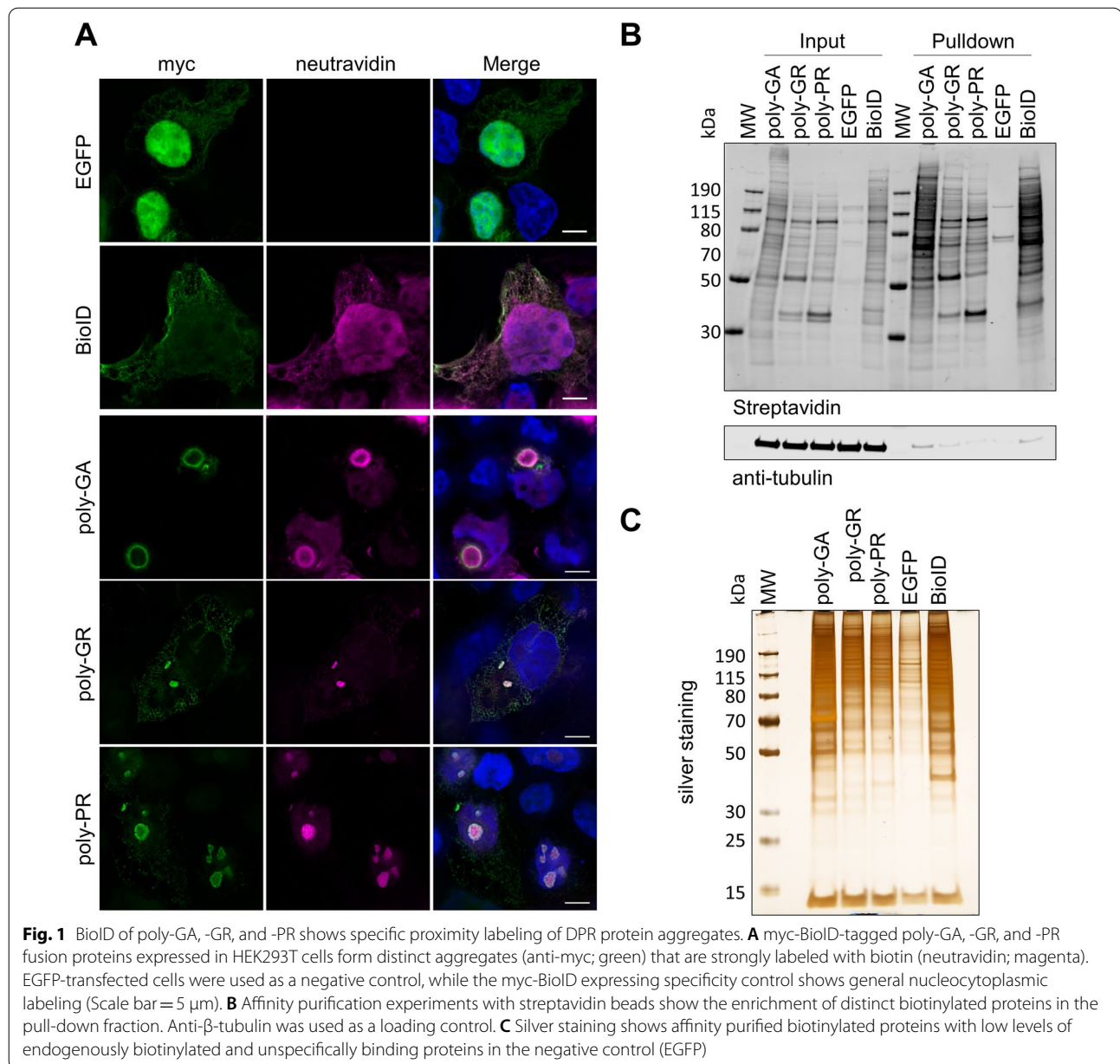
#### Statistical analysis

Quantitative data is presented as mean ± SD. Statistical comparisons between multiple experimental groups were performed using Kruskal–Wallis test followed by post hoc pairwise comparison between control and experimental groups via a Dunn's multiple comparison test. Statistical analysis was performed using GraphPad Prism software (V 9.2.0).

## Results

### Proximity-dependent biotin identification (BioID) of DPR-associated proteomes in HEK293T cells

The BioID assay is based on the expression of a promiscuous biotin ligase fusion protein that catalyzes the biotinylation of proximate lysine residues, to allow for the identification of proximal and interacting proteins in the context of living mammalian cells [80]. Poly-GA, poly-GR, and poly-PR encoding sequences (as 100 repeats) were generated via DNA synthesis and cloned as a C-terminal fusion connected via a flexible linker (GGGSGGGSGGGGS) into a myc-BirA\* plasmid encoding the promiscuous R118G mutant of the *E. coli* biotin ligase BirA (Fig. 1A)[80]. We selected the original BirA\* biotin ligase with slow labeling kinetics, now also commonly referred to as BioID, over more processive variants such as TurboID that were developed to efficiently label proteins within cellular components [9], since we aimed to preferentially label protein components associated with insoluble aggregates instead of soluble proteins. To validate the approach via immunocytochemistry, HEK293T cells were transfected with BioID-DPR<sub>x100</sub> expression and control constructs and incubated for 24 h to allow for the formation of protein aggregates. After incubation with 50 μM biotin to induce biotinylation of proximate proteins, immunostaining with anti-myc antibodies and fluorophore-labeled neutravidin was performed. Myc-BioID-poly-GA formed dense cytoplasmic aggregates consistent with human pathological findings, whereas myc-BioID-poly-GR was observed in both the nucleoli and cytoplasm, and myc-BioID-poly-PR was mainly nucleolar (Fig. 1A). While nuclear and para-nucleolar DPR inclusions are rare in human autopsy brain tissue, these localization patterns are consistent with previous in vitro studies on poly-GR and -PR aggregates using different tags and cell types [85]. These localization patterns suggests that BioID-fusions do not affect the localization of DPRs in cell culture. As a specificity control, we expressed myc-BioID, which showed the expected general nucleocytoplasmic distribution, while the EGFP expression plasmid was used as a negative control. Neutravidin staining demonstrates the colocalization of biotinylated proteins with myc-BioID-DPR<sub>x100</sub> and myc-BioID



proteins, whereas cells transfected with EGFP were negative for biotinylation.

To affinity-purify proximity-biotinylated proteins, cells were incubated with biotin as described above, washed thoroughly in PBS and lysed under harsh denaturing conditions in 8 M urea buffer to solubilize protein aggregates, as previously established for TDP-43 aggregates [12]. Western blots with fluorescent neutravidin showed distinct patterns of proximity-dependent biotinylation in myc-BioID-DPR cell lysates and pull-down samples, as compared to low abundant endogenously biotinylated proteins present in the EGFP-transfected negative

control (Fig. 1B). Silver staining was used to confirm selective enrichment of purified biotinylated proteins over nonspecifically binding proteins in the negative control (Fig. 1C).

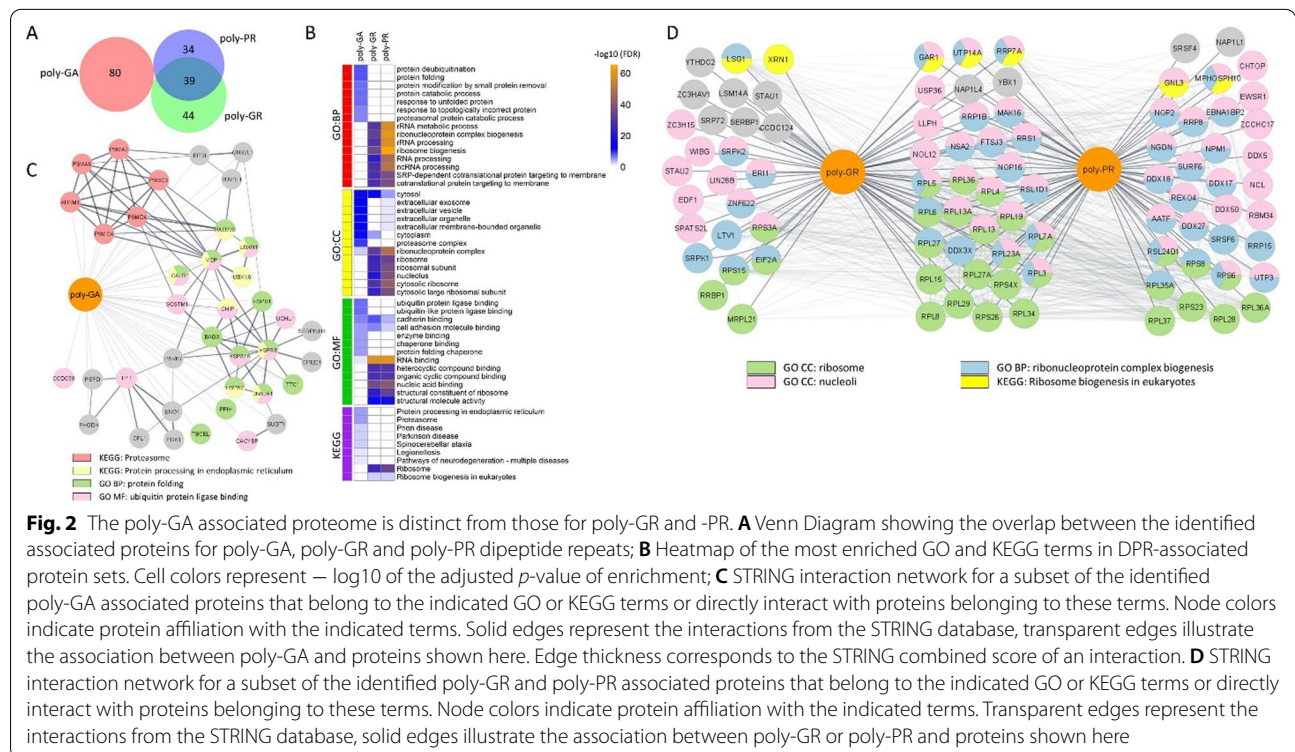
For proteomic analysis of DPR-associated biotinylated proteins, streptavidin bead-bound proteins were digested with trypsin, and the obtained peptides were analyzed by data independent acquisition mass spectrometry (DIA LC-MS/MS). For each of the studied constructs or controls three biological replicates were prepared. Principal component analysis of the samples highlights tight clustering of the proximity proteomes of arginine-containing

DPRs and poly-GA, that were well separated along the PC1 axis (Additional file 1: Supplementary Fig. 1A). Principal component 2 separated poly-GR from poly-PR and poly-GA from myc-BioID negative controls (Additional file 1: Supplementary Fig. 1A). By applying the stringent criteria discussed in the methods section, we have identified 80 proteins associated with poly-GA, 83 proteins associated with poly-GR and 73 proteins associated with poly-PR (Fig. 2A, Additional file 2: Supplementary Table 1). Notably, no common interactors for the arginine-rich DPRs vs. poly-GA aggregates were identified in our analysis (Fig. 2A).

**Poly-GR and poly-PR proximity proteomes overlap and are highly enriched for ribosomal and nucleolar proteins**

Analysis of the GO terms and KEGG pathway enrichment was performed in each of the obtained sets of DPR interactors, showing distinct functional classifications for the poly-GA interactome vs. the strongly overlapping arginine-rich DPRs (Fig. 2B). For both poly-GR and poly-PR associated proteins the most enriched GO terms were ribosomal function or biogenesis (Fig. 2B, D). Proteins assigned to this category include ribosomal proteins, ribosome biogenesis factors, and other nucleoli resident proteins. Other proteins associated with poly-GR and poly-PR include RNA-binding proteins associated with membrane-less organelles that not only include

nucleoli but also stress granules. These findings are in good agreement with the observed cellular localization of these DPRs, as well as with previous studies that reported the association of poly-GR and poly-PR with ribosomal and nucleolar proteins using different experimental models and paradigms [32, 46, 49, 64]. While many of these associated proteins were shared between poly-GR and poly-PR (i.e. RPL4, RPL5, RPL6 etc.), others were exclusively found in poly-GR (i.e. LTV1, STAU2 etc.) or poly-PR (i.e. NPM1, EWSR1, etc.) associated proteomes (Fig. 2D; Additional file 1: Supplementary Fig. 1C and D, Additional file 2: Supplementary Table 1). Several of these proteins identified in our proximity proteomics study exhibited a potential functional connection to C9orf72 pathological features. The *Drosophila* ortholog of double-stranded RNA-binding protein Staufen homolog 2 (STAU2) shows nuclear accumulation when C9orf72-associated arginine-rich dipeptide repeats are expressed, as an important pathological feature in neurons [44]. Nucleophosmin (NPM1) has been shown to disperse from nucleoli and disrupt its role in organizing ribosomal proteins and RNAs within the nucleolus upon poly-PR expression, suggesting a direct mechanistic link to protein synthesis defects in c9FTD/ALS models [94]. Rare genetic variants of the RNA-binding protein EWS (EWSR1) in ALS patients cause the formation of cytoplasmic aggregates and this protein has also been



observed to co-aggregate in FTLD cases with FUS pathology, suggesting a potential role in the FTD/ALS disease process [15, 69].

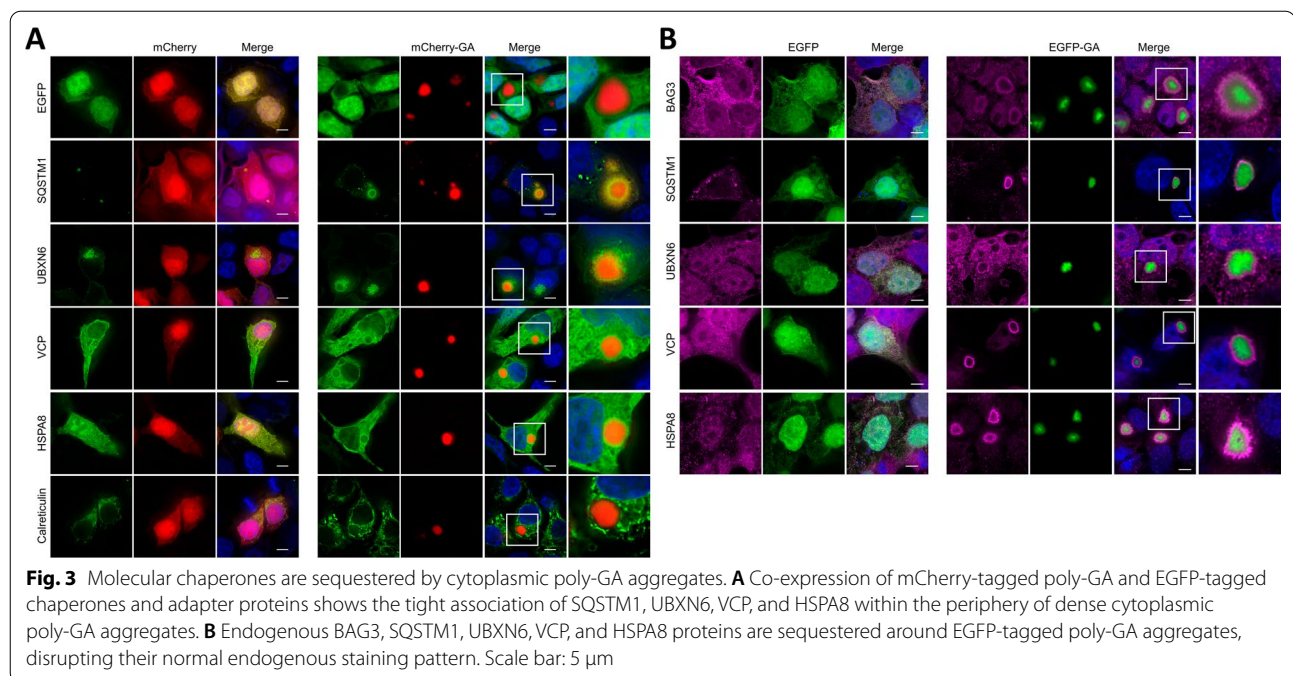
#### **Poly-GA associates with a network of heat shock proteins and other chaperones and co-chaperones**

Comparison of the poly-GA associated proteins identified in this study with previously published datasets [8, 60, 64] shows some limited overlap but also identifies 71 novel poly-GA specific interactors, probably due to different experimental approaches used (Additional file 1: Supplementary Fig. 2). The fact that we found no overlap with poly-GR and -PR associated proteins reflects the fundamental differences in the biophysical properties of these compact aggregates formed by small, aliphatic, and uncharged amino acids [21]. In contrast to the association of the poly-GR and poly-PR interactomes with the KEGG pathway terms “ribosome” and “ribosome biogenesis”, the poly-GA-associated protein set was enriched for the KEGG pathway term “proteasome”, “protein processing in endoplasmic reticulum” as well as neurodegenerative disease pathways including “Parkinson’s disease” and “spinocerebellar ataxia” that are characterized by detergent-insoluble  $\alpha$ -synuclein or prevalent polyglutamine (poly-Q) aggregates, respectively (Fig. 2B). The identified proteasomal proteins PSMA2, PSMA6, PSMC3, PSMC4 and PSMD4, as well as proteasomal ubiquitin receptor ADRM1 (Fig. 2C), are in line with cryo-electron tomography studies showing the accumulation of 26S proteasomes in poly-GA aggregates [26]. The most enriched functional GO Biological Process terms for poly-GA associated proteins were “protein folding” and “ubiquitin protein ligase binding” (Fig. 2B). These GO terms encompass calreticulin (CALR), which was the most enriched protein in poly-GA samples when compared to myc-BioID specificity controls (Additional file 1: Supplementary Fig. 1B). Calreticulin is the ER resident chaperone that facilitates glycoprotein folding in the ER lumen and is involved in ER-associated degradation (ERAD) of misfolded proteins [37]. Importantly, another highly enriched poly-GA associated protein in this study was the autophagy receptor SQSTM1/p62, which is a well-known poly-GA interactor and robust neuropathological screening marker for DPR pathology in c9FTD/ALS cases [57, 60, 67]. Other poly-GA associated proteins from these functional categories include small heat shock proteins from the HSP70-family of chaperones HSPA1A/HSP70-1, HSPA2/HSP70-2 and HSPA8/HSC70, small heat shock protein HSPB1/HSP27, co-chaperones DNAJA1 and BAG3, as well as the key ERAD and autophagy regulator valosin-containing protein/ATPase p97 subunit (VCP/p97) and known poly-GA associated protein RAD23B/HR23B (Fig. 2C) [60, 78, 101]. Along with VCP that

facilitates the degradation of aberrant proteins by segregating them from organelles or large protein complexes [97], the VCP adaptors UBXN1/SAKS1 and UBXN6/UBXD1 were also found to be associated with poly-GA. For our validation experiments we focused on how this network of molecular chaperones and co-chaperones associate with poly-GA in response to the formation of cytoplasmic poly-GA protein aggregates.

#### **Molecular chaperones are sequestered by poly-GA aggregates in cell culture**

To better understand the relationship between poly-GA aggregates and components of cellular protein folding, quality control, and protein degradation pathways, we investigated their co-localization in cell culture using two complementary methods. In an antibody-independent approach, HEK293T cells were co-transfected with constructs for mCherry-tagged poly-GA and EGFP-tagged chaperones and co-chaperones (Fig. 3A). mCherry-poly-GA forms compact cytoplasmic aggregates, with co-localization of EGFP-tagged interactors presenting with halo-like staining that surrounds the inclusions in single optical sections, as observed from 3D deconvolved image stacks using high resolution fluorescence microscopy. Strong overlap was found for SQSTM1, while a more peripheral association was observed for co-expressed UBXN6, HSPA8 and VCP, whereas CALR showed a more distal association (Fig. 3A). In our second approach, we investigated potential sequestration of cellular proteins into poly-GA aggregates by expressing EGFP-tagged poly-GA and immunostaining fixed cells for endogenous protein candidates (Fig. 3B). High resolution fluorescence microscopy demonstrates a very similar staining pattern of endogenous proteins as compared to the EGFP-tagged fusion proteins, with BAG3, SQSTM1, UBXN6, VCP, and HSPA8 localized at the periphery of the cytoplasmic poly-GA aggregates. Their sequestration to the poly-GA inclusions and loss of normal cellular localization suggests potential defects in the normal cellular functions of these proteins (Fig. 3B). Of note, we observed a concentric staining pattern for both exogenous EGFP-tagged and endogenous interactors, with SQSTM1 staining overlapping with the periphery of the poly-GA aggregates, while HSPA8, UBXN6 and especially VCP appeared more peripheral and separated from the poly-GA aggregate. This spatial pattern is consistent with a role for UBXN6 acting as an adaptor for recruiting VCP to poly-GA aggregates that are decorated by SQSTM1, similar to its role as a VCP adaptor for aggresomes and poly-Q containing aggregates [68]. While the GFP-tag introduces lysine residues that may be directly ubiquitinated, previous studies have shown that expression of lysine-free HA-tagged poly-GA in cells



leads to formation of poly-GA aggregates that are both ubiquitin- and p62-positive [96, 100]. To exclude a tag-specific artifact, we repeated co-localization experiments using expression construct encoding 2xHA-tagged poly-GA that lacks any lysine residues and found a similar association with VCP and HSPA8 (Additional file 1: Supplementary Fig. 3).

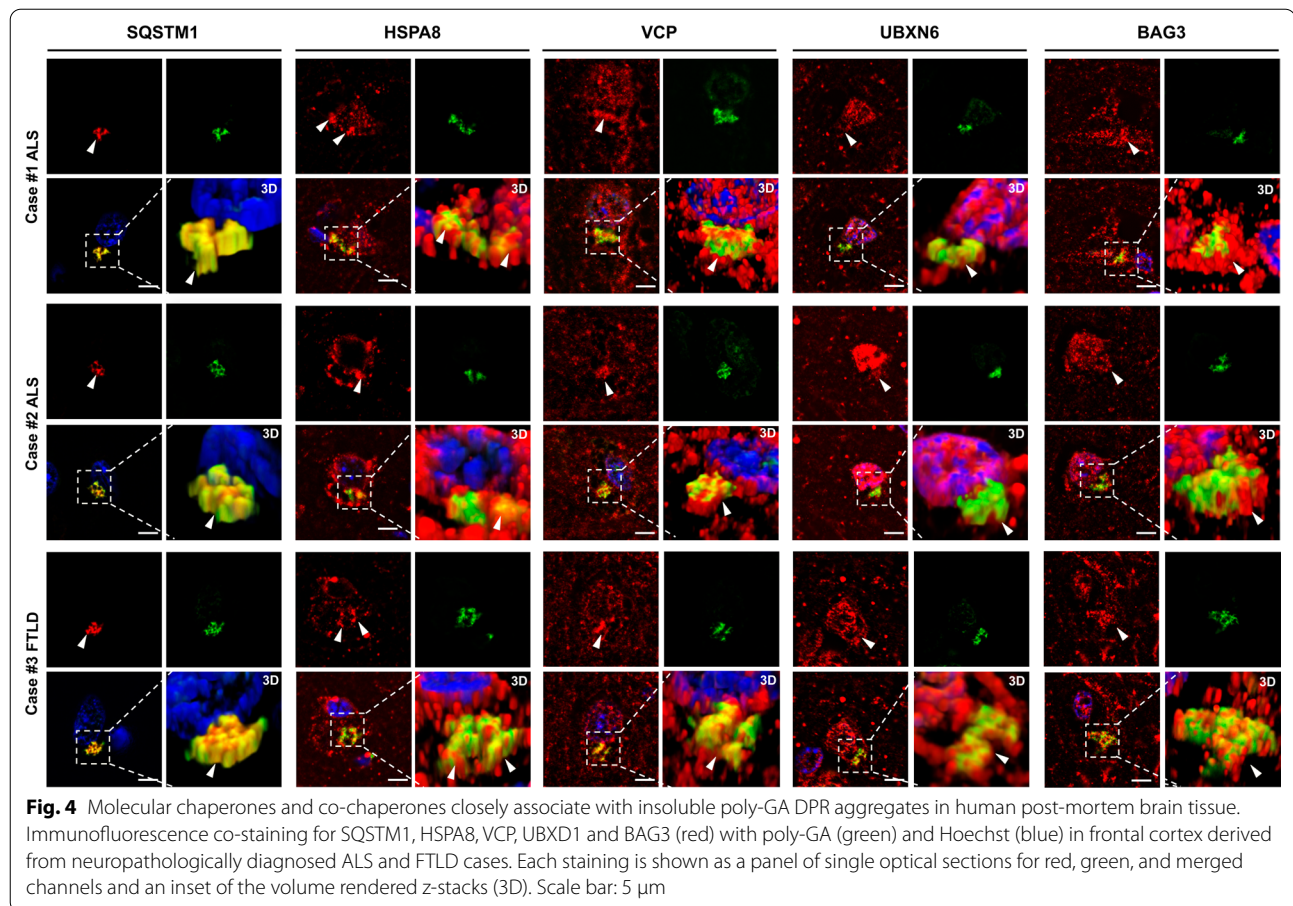
#### UBXN6, HSPA8, and VCP co-localize with SQSTM1-positive poly-GA aggregates in the brain of c9FTD/ALS cases

To validate our *in vitro* findings and establish their relevance for c9FTD/ALS pathogenesis, we determined whether these chaperones localize to poly-GA pathology in human patient brains. For this purpose, we performed stringent fluorescence double-labeling experiments in frontal cortices selected c9FTD/ALS cases with C9orf72 repeat expansion pathology from the Mayo Clinic brain bank (Table 1). High resolution fluorescence imaging was performed using a 100 $\times$  objective to acquire z-series of optical sections for deblurring and 3D image reconstructions. Great care was taken to block autofluorescence and adjust imaging parameters to prevent overexposure. Using these stringent conditions, we observed co-localization patterns that closely matched results from our cell culture model, except that poly-GA aggregates appear round and smooth in cells, probably due to the fast kinetics of overexpression and aggregation, while their shape in brain tissue was often star-shaped or peri-nuclear crescent-shaped and appeared irregular as described before [85] (Fig. 4). Similar to the close association observed in

cells, SQSTM1 showed highly overlapping localization with poly-GA, visible as yellow pixels in merged images (Fig. 4), corroborating their diagnostic utility in the neuropathological screening and diagnosis of c9FTD/ALS. In addition to the optical sections, here we present volume rendered z-stacks to show the true nature of their co-localization within cells in 3D. Confirming our cell culture studies, we found that HSPA8, VCP, UBXN6 and BAG3 showed intimate co-localization and permeated cytoplasmic frontal cortex poly-GA aggregates, suggesting that they are recruited to ubiquitinated and SQSTM1-positive DPR aggregates. A similar staining pattern was observed in the temporal cortex and hippocampal dentate gyrus of c9FTD/ALS cases (Additional file 1: Supplementary Fig. 4 and 5, respectively), except that colocalization with BAG3 was not observed in all cases.

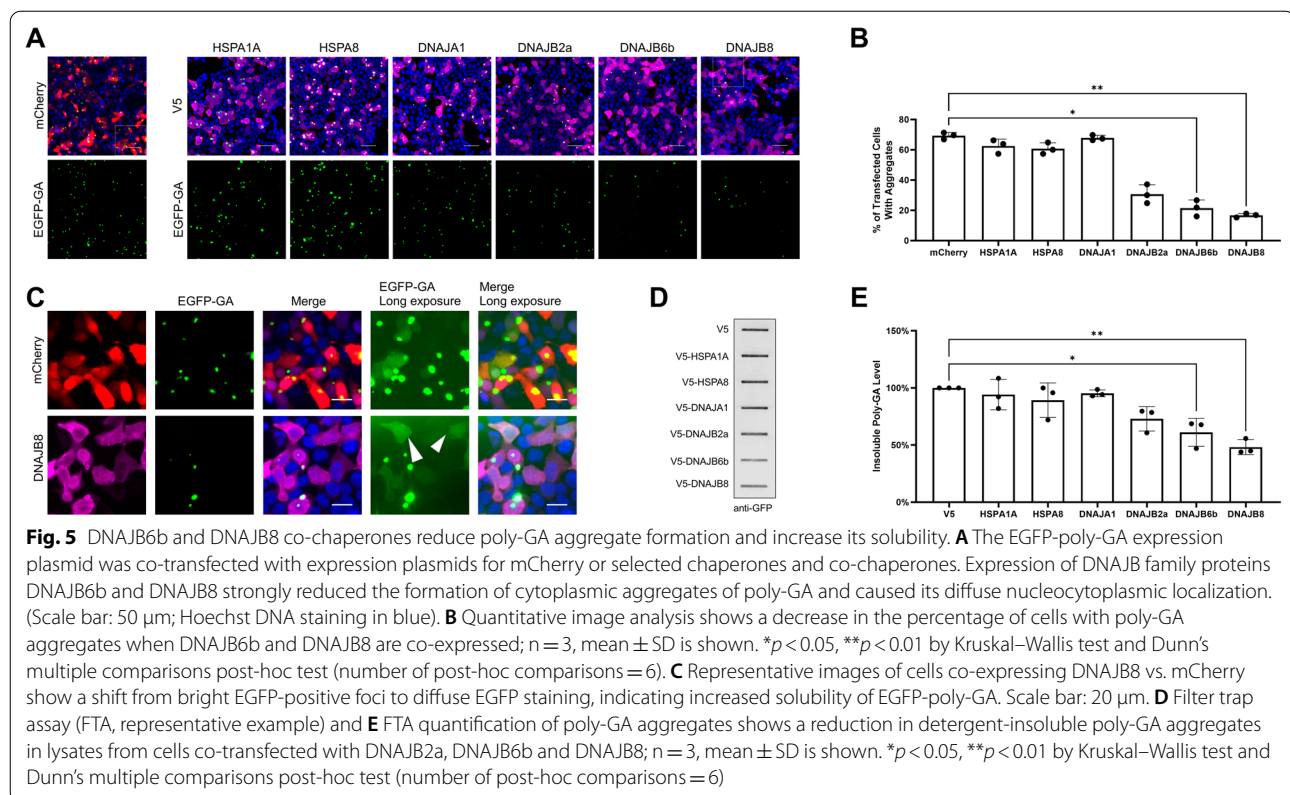
#### DNAJB protein family co-chaperones reduce the formation of poly-GA aggregates

HSP40/DNAJ family proteins acting as co-chaperones for HSC/HSP-70 ATPases have been shown to protect against neurodegeneration caused by misfolding and aggregation of various proteins, including poly-Q expanded proteins, amyloid- $\beta$ ,  $\alpha$ -synuclein, tau, Parkin, SOD1, and TDP-43 [99]. In our proximity proteomics data set we identified DNAJA1 as a novel poly-GA associated protein (Fig. 2C). This largest chaperone family consists of the DNAJA, DNAJB, and DNAJC sub-families with different domain structures. Since its members



are characterized by tissue-specific expression patterns including the CNS, they may not be active in HEK293T cells [99]. In a previous pilot screen of DNAJ family protein for reduction of poly-GA aggregation, we had identified several DNAJB protein family members as potential modifiers of poly-GA aggregate formation (data not shown). Of note, co-chaperones DNAJA1 and DNAJB6 have previously been identified as modulators of poly-Q huntingtin (htt) aggregation in a cellular Huntington's disease model, with the knock-out (KO) of DNAJB6 resulting in a fivefold increase in poly-Q74htt aggregation while a DNAJA1 KO resulted in a fourfold decrease of poly-Q74htt aggregation [79]. DNAJB6 is most closely related to its protein family members DNAJB2 and DNAJB8, which share a broad activity towards different neuropathological aggregates [99]. Both DNAJB6 and DNAJB8 have been shown to prevent the aggregation of pure polyQ peptides in vitro [25]. To investigate the effect of these HSP40/DNAJ family proteins on poly-GA aggregation, we co-transfected HEK293T cells with expression plasmids for EGFP-tagged poly-GA and V5-tagged co-chaperones. We selected candidates for our assays based on our BioID dataset and added DNAJB family proteins

identified in a previous screen as described above. The complementary use of imaging and biochemical assays allowed us to determine and quantify their effect on poly-GA aggregation and solubility. In the microscopy-based assay, we assessed the presence of EGFP-poly-GA foci vs. soluble protein GA in co-transfected cells. Filter trap assays were used to measure detergent-solubility of poly-GA in the resulting lysates. Expression of the co-chaperones DNAJB6b and DNAJB8 strongly reduced the formation of poly-GA aggregates, whereas DNAJA1 and the chaperones HSPA1A and HSPA8 had no significant effect (Fig. 5A and B). We also observed that DNAJB2a could visibly reduce poly-GA aggregation, although the difference between DNAJB2a and mCherry control conditions did not reach statistical significance (Fig. 5A, B, D and E). HSPA8 showed the strongest colocalization with poly-GA aggregates, while a weaker association is observed for the co-chaperones from the HSPB family. Overexposing images reveal the presence of diffuse EGFP-poly-GA distribution in cells expressing active DNAJB co-chaperones to a much greater extent than in controls, where EGFP-poly-GA predominantly forms round inclusions due to the high propensity of



poly-GA to aggregate (Fig. 5C). In the filter trap assay, we assessed the detergent solubility of poly-GA protein when co-expressed with molecular chaperones. Confirming the results from microscopy, we found a decrease in 2% SDS-insoluble poly-GA aggregates when DNAJB6b and DNAJB8 were co-expressed (Fig. 5D and E). Taken together, our results establish that the same group of co-chaperones from the DNAJB family that reduce poly-Q,  $\alpha$ -synuclein, and TDP-43 aggregation [1, 2, 10, 25], also strongly reduce the formation of insoluble poly-GA aggregates. These findings suggest that current efforts to harness the activity of cellular chaperone networks to target neuropathological aggregates may be used to target poly-GA aggregates in c9FTD/ALS patients [17, 88, 99].

## Discussion

In this study we report that proximity-proteomics is a highly valuable strategy for interrogating the composition and associated proteome of neuropathological inclusions, which allowed us to identify key factors that could be exploited as therapeutic modifiers of DPR pathogenesis in c9FTD/ALS. While most interactome studies employ classical immunoaffinity purification, we have found that proximity-dependent biotin identification (BioID) can be used to profile the composition of detergent-insoluble aggregates, which has led to our previous discovery

of nucleocytoplasmic transport defects associated with TDP-43 pathology [12]. Unlike conventional co-immunoprecipitation approaches in cell lysates, BioID and related methods using biotin ligase variants (e.g. TurboID) or engineered peroxidases (APEX2) allow for spatiotemporal labeling of the components and closely associated proteins of insoluble aggregates in the context of living cells, followed by harsh solubilization conditions (e.g. 8 M urea) and high-affinity biotin-streptavidin purification for mass spectrometry based proteomics [82]. APEX2 is more suitable for capturing the composition of dynamic condensates and has been used for the spatiotemporal characterization of the stress granule proteome, and for evaluating the effect of poly-PR on the stress granule proteome [59]. For poly-GA that forms compact and highly insoluble aggregates composed of amyloid fibrils, conventional affinity purification methods have yielded fewer interactors than for charged arginine-rich poly-GR and -PR [49]. Although the dense nature of myc-BioID-poly-GA aggregates appeared to limit the penetration of anti-myc antibodies, it does not impede proximity labeling with small biotin molecules in living cells, allowing us to identify numerous and novel poly-GA interactors (Fig. 1A).

Our proximity proteomics data for poly-GR and -PR are consistent with the literature, showing enrichment

for nucleolar and ribosomal proteins [32]. Expression of these arginine-rich repeats in cell culture shows a stronger staining of nucleoli than has been reported from human brain tissue, whereas the subcellular distribution of poly-GA aggregates matches human neuropathological findings [85]. While we also discovered novel poly-GR/PR interactors with potential links to c9FTD/ALS pathophysiology as described above and in Fig. 2, in our validation experiments and functional assays we focused on the poly-GA interactome. The highly aggregation prone poly-GA can induce significant neurotoxicity in cellular and animal models of c9FTD/ALS [26, 40, 41, 47, 60, 72, 74, 84]. While poly-GR can recruit TDP-43 into cytoplasmic inclusions [14], poly-GA may promote TDP-43 aggregation more indirectly via inhibition of proteasome mediated protein degradation [41, 73]. Studies in mouse models report poly-GA toxicity causing neuroinflammation and additional defects caused by the sequestration of proteins into insoluble aggregates [41, 47, 84, 100, 101]. For these reasons, interrogating poly-GA interactomes and affected pathways will contribute to a better understanding of c9FTD/ALS relevant disease processes and therapeutic targets [33].

Our validation experiments included overexpression of tagged proteins and immunocytochemistry of endogenous proteins in cell culture (Fig. 3A and B) and immunohistochemistry in patient-derived brain tissue from neuropathologically confirmed c9ALS and c9FTLD autopsy cases. Using high resolution fluorescence microscopy with deconvolved image stacks, we found a very consistent pattern across these experiments, with SQSTM1 showing a very close association and co-localization with poly-GA aggregates, while VCP, its adaptor protein UBXN6 and the chaperones HSPA8 and BAG3 demonstrated close association and permeation of poly-GA inclusion, but not completely overlapping co-localization. These findings not only validate our proximity proteomic interactome results but also suggest a distinct spatial relationship with SQSTM1 decorating ubiquitinated aggregates, while chaperones appear to be sequestered within and towards the periphery of the inclusions. These findings also highlight a specific feature of proximity labeling vs. co-immunoprecipitation of physically associated proteins that allows us to interrogate the molecular environment of protein complexes. While the labeling radius for BioID in endogenous protein complexes has been estimated at approximately 10 nm [42], the use of a flexible linker in the fusion proteins and its high local concentration in aggregates may expand labeling to some extent [43].

The poly-GA interactome was highly enriched for proteins involved in protein folding, ubiquitination, and degradation. STRING pathway analysis showed one

major node group for proteasome components, consistent with the accumulation of cellular proteasomes in poly-GA aggregates [26]. Another major group of nodes in the interactome network is clustered around the ATPase VCP, and its adaptor proteins UBXN1 and UBXN6. This cluster of functionally connected interactors also encompasses the Ub-associated (UBA) domain ubiquitin receptor for proteasomal degradation RAD23B, and the autophagic ubiquitin receptor SQSTM1 [105]. In a murine model of poly-GA pathology and in human *C9orf72* expansion carriers RAD23B was found to be sequestered into poly-GA inclusions, while SQSTM1 is a known reliable marker for DPR pathology in c9FTLD/ALS [58, 101]. Another member of this group is the ER chaperone CALR, which has multiple functions including the regulation of Ca<sup>2+</sup> homeostasis and protein folding, and was found dysregulated in neurological disorders, including ALS [45]. Of note, a study of motor dysfunction in a poly-GA mouse model has shown mobile poly-GA aggregates within neurites, causing altered Ca<sup>2+</sup> influx and synaptic vesicle release [36]. It would be interesting to see whether these defects are mediated via the association of poly-GA with CALR.

Dysfunction of autophagy-related proteins impairs proteostasis and causes neurotoxicity in FTD/ALS, and mutations in both SQSTM1 and VCP can cause ALS and FTD [13]. VCP, in combination with adaptor proteins such as UBXN1 and UBXN6, functions to identify misfolded proteins, extract them from aggregates and damaged mitochondria and lysosomes, and target them for degradation by the proteasome or through autophagy [22, 27, 75]. VCP and its adaptor FAF2 were recently found to mediate the extraction of G3BP1 from stress granules induced by heat stress, leading to their disassembly [29], which establishes an interesting connection between stress granule dynamics and the pathogenesis of proteinopathies [52]. SQSTM1 serves as an autophagy receptor protein that binds both LC3-II and polyubiquitinated proteins, targeting ubiquitinated substrates to autophagosomes for degradation [13]. Taken together, these findings suggest a direct link of poly-GA aggregates to autophagy as a substrate but may also reflect a dysregulation of both major pathways of protein degradation caused by the sequestration of autophagy receptors and proteasomal subunits.

These autophagy-related proteins are functionally connected to another cluster of proteins containing the heat shock proteins HSPA8, HSPA1A, HSPB1, SERPIN H1/HSP47, the co-chaperones BAG3 and DNAJA1, and the E3 ubiquitin ligase CHIP, which targets misfolded chaperone substrates towards proteasomal degradation. Mutations in BAG3, HSPB1, and CHIP have been linked to neurodegenerative diseases [83]. In

addition, we also found ubiquitin C-terminal hydrolase L1 (UCHL1) and Parkinson disease protein 7 (PARK7/DJ-1) that are closely associated with the above-mentioned molecular chaperones in the STRING interaction network and are both linked to Parkinson's disease [7, 51].

Supporting evidence for a disease-relevance of our findings comes from a transcriptomics study that found an induction of a heat shock response caused by C9orf72 pathology in c9FTL/ALS brain tissue relative to both sporadic cases and controls [65]. The upregulated network of transcripts under control of the HSF1 transcription factor includes several poly-GA associated proteins that we have identified in this study, such as BAG3, HSPB1/HSP27, SERPIN H1/HSP47, HSPA1A, but also DNAJB proteins. This study also found a significant upregulation of HSPA1B transcripts in human neurons treated with poly-GA and poly-GR, supporting a role for DPR-specific gain-of-function effects in activating a heat shock response [65].

HSP70 family chaperones play a key role in ATPase mediated correct folding of aberrant protein substrates under normal conditions but also under cellular stress exposure and in neurodegenerative proteinopathies, which has led to development of therapeutic strategies targeting their upregulation [28]. HSP70/HSC70 proteins are also regulated by their association with co-chaperones and other factors. Notably, the ALS/FTD risk factor UBQLN2 can recognize ubiquitinated HSP70 to facilitate the clearance of poly-GA aggregates, thereby alleviating neurotoxicity in a poly-GA animal model [100]. Here we found an association with the C-terminal HSC70-interacting protein (CHIP), which acts as a chaperone dependent E3 ligase that ubiquitinates unfolded proteins and can bind to HSC70 and HSP70, and can switch chaperone activity from protein folding to protein degradation [20]. Another regulatory co-chaperone identified here is BAG3, which is implicated in rerouting UPS substrates to BAG3-mediated selective macroautophagy. BAG3 in concert with HSP70/HSC70 as well as the ubiquitin receptor p62/SQSTM1 specifically targets aggregation-prone proteins to autophagic degradation under conditions of cellular stress and in the context of aging and neurodegenerative diseases [89]. We also identified DNAJA1, which belongs to a large family of DNAJ/HSP40 co-chaperones that target misfolded target protein substrates to specific HSP70 chaperones for refolding. Their tissue-specific expression, high substrate specificity, and potent activity towards targeting misfolded disease proteins makes them an attractive target for therapeutic interventions of neurodegenerative disorders [4]. Our identification of this poly-GA associated network of functionally related HSP70/HSC70

chaperones and co-chaperones suggest its critical role in protein aggregate clearance in c9FTD/ALS.

This work also reveals a novel role of the DNAJB family of co-chaperones that have been previously shown to reduce poly-Q and  $\alpha$ -synuclein aggregation [1, 19, 25, 79] and modulate their pathology in animal models of Parkinson's disease and Huntington's disease [2, 38], in strongly reducing the formation of insoluble poly-GA aggregates (Fig. 5A and B). This subfamily of DNAJB proteins comprises the closely related DNAJB2a, DNAJB6b and DNAJB8 proteins, which were the most efficient at reducing poly-Q aggregation [31]. While these proteins were not identified in the proximity proteome in HEK293T cells, they are normally expressed in a tissue specific manner and we selected them for further investigation due to their activity towards poly-GA aggregation in a screen and their well-documented activity towards neuropathological inclusions in the literature [99]. Recessive mutations in the gene encoding the neuronal DNAJB2/HSJ1 protein can result in distal hereditary motor neuronopathy, Charcot-Marie-Tooth disease type 2, or spinal muscular atrophy/juvenile Parkinsonism [99]. DNAJB6/MRJ is ubiquitously expressed but most abundantly localized within the brain and in muscle tissue, with mutations causing dominant limb-girdle muscular dystrophy [99]. In patients carrying DNAJB6 mutations this anti-aggregation property is reduced, and they present with myofibrillar inclusions positive for ubiquitin, SQSTM1 and TDP-43, suggesting defective protein clearance [81]. Our results suggest that therapeutic efforts to target the activity of DNAJB6 and related co-chaperones in synucleinopathies and poly-Q disorders may also be beneficial for c9FTD/ALS patients, potentially targeting both TDP-43 and poly-GA aggregation. It remains to be observed whether the broad target specificity of these DNAJB family co-chaperones results from recognizing common structural features on the misfolded protein substrates or shared interactors of these divergent neuropathological aggregates [4].

While this manuscript was in preparation, a related study based on a similar strategy was published [8]. Although some of our results overlap, including the identification of VCP in the poly-GA interactome, we also identified numerous additional poly-GA associated proteins, including VCP adapters, molecular chaperones and co-chaperones, and SQSTM1, a highly reliable marker for poly-GA pathology *in vitro* and in autopsy tissue. This difference may be due to our method that we have optimized for the study of neuropathological inclusions, such as using more stringent lysis conditions in our study (8 M urea instead of 0.2% SDS + 2% Triton X-100) for solubilizing detergent-insoluble poly-GA aggregates and associated proteins, which allows us to also identify

insoluble co-depositing proteins involved in c9FTD/ALS pathogenesis.

Of note, therapeutic strategies targeting poly-GA have shown promising results in C9orf72 mouse models. Active poly-GA vaccination by immunizing a C9orf72 mouse model with a poly-GA fusion protein markedly reduced neuroinflammation, motor deficits, cytoplasmic TDP-43 mislocalization and CSF levels of neurofilament light chain, the latter of which is a reliable biomarker of neurodegeneration [103]. Passive immunotherapy based on injecting C9orf72-BAC mice with a human anti-GA antibody reduced not only poly-GA, but also -GP, and -GR aggregates, which subsequently improved behavior and survival, whilst also decreasing neurodegenerative read-outs [71]. Taken together, these data suggest that immunotherapies or other strategies primarily targeting poly-GA pathology may be a suitably viable therapeutic approach for c9FTD/ALS [33]. Neuropathological and biomarker studies suggest that targeting early prodromal DPR pathology may prevent the later onset of symptoms and the appearance of TDP-43 pathology and resultant neurodegeneration [5, 23, 50, 93].

While this work and other studies provide evidence for poly-GA aggregates causing defects in protein degradation, it remains unclear how poly-GA pathology triggers neuroinflammation in mouse models and potentially c9FTD/ALS in human brains [47, 71, 84, 103]. Reduced C9orf72 protein levels [104], the presence of RNA repeat pathology, and the co-aggregation of multiple DPRs as separate molecules or chimeric peptides [61] are expected to contribute to the complexity of DPR pathologies and their spectrum of clinicopathologic presentations. Future studies in vertebrate animal models that combine multiple aspects of C9orf72 neuropathology, neuroinflammation and neurodegeneration and studies utilizing the rich resource of diagnostically confirmed human brain tissue will be required to obtain a more complete picture of the timeline and specific contributions of DPR pathologies in the disease process.

## Supplementary Information

The online version contains supplementary material available at <https://doi.org/10.1186/s40478-022-01322-x>.

**Additional file 1.** Supplementary Fig. 1, 2, 3, 4, 5.

**Additional file 2.** Supplementary Table 1.

## Acknowledgements

We thank the patients and their families for participating in and contributing to these research studies. We also thank Dr. Yongjie Zhang and Monica Castanedes Casey for expert advice with poly-GA IHC and the Neuropathology and Microscopy lab for providing slides with autopsy brain tissue. We thank Drs. Noboru Mizushima, Hemmo Meyer, Nico Dantuma, Harm Kampinga and Michael Davidson for providing the plasmid constructs used in this study.

We thank the patients and their families for their generous donation of brain samples for research.

## Authors' contributions

WR conceptualized and supervised the research; FL and DM planned experiments; FL performed proteomic experiments; DM analyzed and interpreted proteomics data; FL performed biochemical and cell culture experiments; MW performed tissue staining; DD selected cases and provided expertise for tissue staining; MS and BP performed mass spectrometry and provided expertise with data analysis; YW, SV-T, and BR contributed critical assistance and materials; WR, FL, and DM wrote the manuscript, with critical input from MW. BO provided clinical information. All authors read and approved the final manuscript.

## Funding

WR was supported by grants from the National Institutes of Health (NIH R33 NS110960) and the US Department of Defense (W81XWH-19-1-0193). DM was supported by the Audrey Lewis Young Investigator Award from the CureSMA foundation. DWD was supported by NIH awards: P01 NS084974 and P30 AG062677, as well as the Rainwater Charitable Foundation and the Robert E. Jacoby Professorship. The Proteomics Core at the University of California Davis was supported by the Howard Hughes Medical Institute (HHMI).

## Availability of data and materials

Raw proteomic data files along with the Spectronaut search results, quantification and statistical analysis of proteomic data were submitted to ProteomeXchange Consortium via MassIVE mass spectrometry data repository (MassIVE identifier MSV000088581, ProteomeXchange identifier PXD030490).

## Declarations

### Ethics approval and consent to participate

All donors had provided written informed consent for the use of autopsy material and of clinical and genetic information for research purposes.

### Competing interests

The authors declare no conflict of interest.

### Author details

<sup>1</sup>Department of Neuroscience, Mayo Clinic, Jacksonville, FL, USA. <sup>2</sup>Department of Ophthalmology, The Second Hospital of Jilin University, Changchun, China. <sup>3</sup>Department of Neurology, The First Affiliated Hospital of China Medical University, Shenyang, Liaoning, China. <sup>4</sup>Proteomics Core, University of California Davis, Davis, CA, USA. <sup>5</sup>Department of Neurology, Mayo Clinic, Jacksonville, FL, USA.

Received: 24 January 2022 Accepted: 25 January 2022

Published online: 14 February 2022

## References

1. Aprile FA, Kallstig E, Limorenko G, Vendruscolo M, Ron D, Hansen C (2017) The molecular chaperones DNAJB6 and Hsp70 cooperate to suppress alpha-synuclein aggregation. *Sci Rep* 7:9039. <https://doi.org/10.1038/s41598-017-08324-z>
2. Arkan S, Ljungberg M, Kirik D, Hansen C (2021) DNAJB6 suppresses alpha-synuclein induced pathology in an animal model of Parkinson's disease. *Neurobiol Dis* 158:105477. <https://doi.org/10.1016/j.nbd.2021.105477>
3. Ash PE, Bieniek KF, Gendron TF, Caulfield T, Lin WL, DeJesus-Hernandez M, van Blitterswijk MM, Jansen-West K, Paul JW 3rd, Rademakers R et al (2013) Unconventional translation of C9ORF72 GGGGCC expansion generates insoluble polypeptides specific to c9FTD/ALS. *Neuron* 77:639–646. <https://doi.org/10.1016/j.neuron.2013.02.004>
4. Ayala Mariscal SM, Kirstein J (2021) J-domain proteins interaction with neurodegenerative disease-related proteins. *Exp Cell Res* 399:112491. <https://doi.org/10.1016/j.yexcr.2021.112491>
5. Baborie A, Griffiths TD, Jaros E, Perry R, McKeith IG, Burn DJ, Masuda-Suzukake M, Hasegawa M, Rollinson S, Pickering-Brown S et al (2015)

- Accumulation of dipeptide repeat proteins predates that of TDP-43 in frontotemporal lobar degeneration associated with hexanucleotide repeat expansions in C9ORF72 gene. *Neuropathol Appl Neurobiol* 41:601–612. <https://doi.org/10.1111/nan.12178>
6. Boeynaems S, Bogaert E, Kovacs D, Konijnenberg A, Timmerman E, Volkov A, Guharoy M, De Decker M, Jaspers T, Ryan VH et al (2017) Phase separation of C9orf72 dipeptide repeats perturbs stress granule dynamics. *Mol Cell* 65(1044–1055):e1045. <https://doi.org/10.1016/j.molcel.2017.02.013>
  7. Bonifati V, Rizzu P, van Baren MJ, Schaap O, Breedveld GJ, Krieger E, Dekker MC, Squitieri F, Ibanez P, Joosse M et al (2003) Mutations in the DJ-1 gene associated with autosomal recessive early-onset parkinsonism. *Science* 299:256–259. <https://doi.org/10.1126/science.1077209>
  8. Bozic J, Motaln H, Janez AP, Markic L, Tripathi P, Yamoah A, Aronica E, Lee YB, Heilig R, Fischer R et al (2021) Interactome screening of C9orf72 dipeptide repeats reveals VCP sequestration and functional impairment by polyGA. *Brain*. <https://doi.org/10.1093/brain/awab300>
  9. Branon TC, Bosch JA, Sanchez AD, Udeshi ND, Svinikina T, Carr SA, Feldman JL, Perrimon N, Ting AY (2018) Efficient proximity labeling in living cells and organisms with TurboID. *Nat Biotechnol* 36:880–887. <https://doi.org/10.1038/nbt.4201>
  10. Chen HJ, Mitchell JC, Novoselov S, Miller J, Nishimura AL, Scotter EL, Vance CA, Cheetham ME, Shaw CE (2016) The heat shock response plays an important role in TDP-43 clearance: evidence for dysfunction in amyotrophic lateral sclerosis. *Brain* 139:1417–1432. <https://doi.org/10.1093/brain/aww028>
  11. Choi M, Chang CY, Clough T, Broudy D, MacLean B, Vitek O (2014) MSstats: an R package for statistical analysis of quantitative mass spectrometry-based proteomic experiments. *Bioinformatics* 30:2524–2526. <https://doi.org/10.1093/bioinformatics/btu305>
  12. Chou CC, Zhang Y, Umoh ME, Vaughan SW, Lorenzini I, Liu F, Sayegh M, Donlin-Asp PG, Chen YH, Duong DM et al (2018) TDP-43 pathology disrupts nuclear pore complexes and nucleocytoplasmic transport in ALS/FTD. *Nat Neurosci* 21:228–239. <https://doi.org/10.1038/s41593-017-0047-3>
  13. Chua JP, De Calbiac H, Kabashi E, Barmada SJ (2021) Autophagy and ALS: mechanistic insights and therapeutic implications. *Autophagy*. <https://doi.org/10.1080/15548627.2021.1926656>
  14. Cook CN, Wu Y, Odeh HM, Gendron TF, Jansen-West K, Del Rosso G, Yue M, Jiang P, Gomes E, Tong J et al (2020) C9orf72 poly(GR) aggregation induces TDP-43 proteinopathy. *Sci Transl Med*. <https://doi.org/10.1126/scitranslmed.abb3774>
  15. Couthouis J, Hart MP, Erion R, King OD, Diaz Z, Nakaya T, Ibrahim F, Kim HJ, Mojsilovic-Petrovic J, Panossian S et al (2012) Evaluating the role of the FUS/TLS-related gene EWSR1 in amyotrophic lateral sclerosis. *Hum Mol Genet* 21:2899–2911. <https://doi.org/10.1093/hmg/dd1116>
  16. Coyne AN, Zaepfel BL, Hayes L, Fitchman B, Salzberg Y, Luo EC, Bowen K, Trost H, Aigner S, Rigo F et al (2020) G4C2 repeat RNA initiates a POM121-mediated reduction in specific nucleoporins in C9orf72 ALS/FTD. *Neuron*. <https://doi.org/10.1016/j.neuron.2020.06.027>
  17. Cristofani R, Crippa V, Vezzoli G, Rusmini P, Galbiati M, Cicardi ME, Meroni M, Ferrari V, Tedesco B, Piccolella M et al (2018) The small heat shock protein B8 (HSPB8) efficiently removes aggregating species of dipeptides produced in C9ORF72-related neurodegenerative diseases. *Cell Stress Chaperones* 23:1–12. <https://doi.org/10.1007/s12192-017-0806-9>
  18. DeJesus-Hernandez M, Mackenzie IR, Boeve BF, Boxer AL, Baker M, Rutherford NJ, Nicholson AM, Finch NA, Flynn H, Adamson J et al (2011) Expanded GGGGCC hexanucleotide repeat in noncoding region of C9ORF72 causes chromosome 9p-linked FTD and ALS. *Neuron* 72:245–256. <https://doi.org/10.1016/j.neuron.2011.09.011>
  19. Deshayes N, Arkan S, Hansen C (2019) The molecular chaperone DNAJB6, but not DNAJB1, suppresses the seeded aggregation of alpha-synuclein in cells. *Int J Mol Sci*. <https://doi.org/10.3390/ijms20184495>
  20. Dickey CA, Patterson C, Dickson D, Petrucelli L (2007) Brain CHIP: removing the culprits in neurodegenerative disease. *Trends Mol Med* 13:32–38. <https://doi.org/10.1016/j.molmed.2006.11.003>
  21. Freibaum BD, Taylor JP (2017) The role of dipeptide repeats in C9ORF72-related ALS-FTD. *Front Mol Neurosci* 10:35. <https://doi.org/10.3389/fnmol.2017.00035>
  22. Ganji R, Mukkavalli S, Somanji F, Raman M (2018) The VCP-UBXN1 complex mediates triage of ubiquitylated cytosolic proteins bound to the BAG6 complex. *Mol Cell Biol*. <https://doi.org/10.1128/MCB.00154-18>
  23. Gendron TF, Chew J, Stankowski JN, Hayes LR, Zhang YJ, Prudencio M, Carlomagno Y, Daugherty LM, Jansen-West K, Perkerson EA et al (2017) Poly(GP) proteins are a useful pharmacodynamic marker for C9ORF72-associated amyotrophic lateral sclerosis. *Sci Transl Med*. <https://doi.org/10.1126/scitranslmed.aai7866>
  24. Gendron TF, Petrucelli L (2018) Disease mechanisms of C9ORF72 repeat expansions. *Cold Spring Harb Perspect Med*. <https://doi.org/10.1101/cshperspect.a024224>
  25. Gillis J, Schipper-Krom S, Juenemann K, Gruber A, Coolen S, van den Nieuwendijk R, van Veen H, Overkleef H, Goedhart J, Kampinga HH et al (2013) The DNAJB6 and DNAJB8 protein chaperones prevent intracellular aggregation of polyglutamine peptides. *J Biol Chem* 288:17225–17237. <https://doi.org/10.1074/jbc.M112.421685>
  26. Guo Q, Lehmer C, Martinez-Sanchez A, Rudack T, Beck F, Hartmann H, Perez-Berlanga M, Frottin F, Hipp MS, Hartl FU et al (2018) In situ structure of neuronal C9orf72 Poly-GA aggregates reveals proteasome recruitment. *Cell* 172(696–705):e612. <https://doi.org/10.1016/j.cell.2017.12.030>
  27. Guo X, Qi X (2017) VCP cooperates with UBXD1 to degrade mitochondrial outer membrane protein MCL1 in model of Huntington's disease. *Biochim Biophys Acta Mol Basis Dis* 1863:552–559. <https://doi.org/10.1016/j.bbadis.2016.11.026>
  28. Gupta A, Bansal A, Hashimoto-Torii K (2020) HSP70 and HSP90 in neurodegenerative diseases. *Neurosci Lett* 716:134678. <https://doi.org/10.1016/j.neulet.2019.134678>
  29. Gwon Y, Maxwell BA, Kolaitis RM, Zhang P, Kim HJ, Taylor JP (2021) Ubiquitination of G3BP1 mediates stress granule disassembly in a context-specific manner. *Science* 372:eabf6548. <https://doi.org/10.1126/science.abf6548>
  30. Hageman J, Kampinga HH (2009) Computational analysis of the human HSPH/HSPA/DNAJ family and cloning of a human HSPH/HSPA/DNAJ expression library. *Cell Stress Chaperones* 14:1–21. <https://doi.org/10.1007/s12192-008-0060-2>
  31. Hageman J, Rujano MA, van Waarde MA, Kakkar V, Dirks RP, Govorukhina N, Oosterveld-Hut HM, Lubsen NH, Kampinga HH (2010) A DNAJB chaperone subfamily with HDAC-dependent activities suppresses toxic protein aggregation. *Mol Cell* 37:355–369. <https://doi.org/10.1016/j.molcel.2010.01.001>
  32. Hartmann H, Hornburg D, Czuppa M, Bader J, Michaelsen M, Farny D, Arzberger T, Mann M, Meissner F, Edbauer D (2018) Proteomics and C9orf72 neuropathology identify ribosomes as poly-GR/PR interactors driving toxicity. *Life Sci Alliance* 1:e201800070. <https://doi.org/10.26508/lsa.201800070>
  33. Hautbergue GM, Cleary JD, Guo S, Ranum LPW (2021) Therapeutic strategies for C9orf72 amyotrophic lateral sclerosis and frontotemporal dementia. *Curr Opin Neurol*. <https://doi.org/10.1097/WCO.00000000000000984>
  34. Hulsen T, de Vlieg J, Alkema W (2008) BioVenn—a web application for the comparison and visualization of biological lists using area-proportional Venn diagrams. *BMC Genom* 9:488. <https://doi.org/10.1186/1471-2164-9-488>
  35. Itakura E, Mizushima N (2011) p62 Targeting to the autophagosome formation site requires self-oligomerization but not LC3 binding. *J Cell Biol* 192:17–27. <https://doi.org/10.1083/jcb.201009067>
  36. Jensen BK, Schuldi MH, McAvooy K, Russell KA, Boehringer A, Curran BM, Krishnamurthy K, Wen X, Westergard T, Ma L et al (2020) Synaptic dysfunction induced by glycine-alanine dipeptides in C9orf72-ALS/FTD is rescued by SV2 replenishment. *EMBO Mol Med* 12:e10722. <https://doi.org/10.15252/emmm.201910722>
  37. Jiang Y, Dey S, Matsunami H (2014) Calreticulin: roles in cell-surface protein expression. *Membranes (Basel)* 4:630–641. <https://doi.org/10.3390/membranes4030630>
  38. Joshi BS, Youssef SA, Bron R, de Bruin A, Kampinga HH, Zuhorn IS (2021) DNAJB6b-enriched small extracellular vesicles decrease polyglutamine aggregation in vitro and in vivo models of Huntington disease. *iScience* 24:103282. <https://doi.org/10.1016/j.isci.2021.103282>
  39. Kanekura K, Yagi T, Cammack AJ, Mahadevan J, Kuroda M, Harms MB, Miller TM, Urano F (2016) Poly-dipeptides encoded by the C9ORF72

- repeats block global protein translation. *Hum Mol Genet* 25:1803–1813. <https://doi.org/10.1093/hmg/ddw052>
40. Khosravi B, Hartmann H, May S, Mohl C, Ederle H, Michaelsen M, Schludi MH, Dormann D, Edbauer D (2017) Cytoplasmic poly-GA aggregates impair nuclear import of TDP-43 in C9orf72 ALS/FTLD. *Hum Mol Genet* 26:790–800. <https://doi.org/10.1093/hmg/ddw432>
  41. Khosravi B, LaClair KD, Riemenschneider H, Zhou Q, Frottin F, Mareljic N, Czuppa M, Farny D, Hartmann H, Michaelsen M et al (2020) Cell-to-cell transmission of C9orf72 poly-(Gly-Ala) triggers key features of ALS/FTD. *EMBO J* 39:e102811. <https://doi.org/10.15252/embj.2019102811>
  42. Kim DI, Birendra KC, Zhu W, Motamedchaboki K, Doye V, Roux KJ (2014) Probing nuclear pore complex architecture with proximity-dependent biotinylation. *Proc Natl Acad Sci U S A* 111:E2453–2461. <https://doi.org/10.1073/pnas.1406459111>
  43. Kim DI, Jensen SC, Noble KA, Kc B, Roux KH, Motamedchaboki K, Roux KJ (2016) An improved smaller biotin ligase for BioID proximity labeling. *Mol Biol Cell* 27:1188–1196. <https://doi.org/10.1091/mbc.E15-12-0844>
  44. Kim ES, Chung CG, Park JH, Ko BS, Park SS, Kim YH, Cha IJ, Kim J, Ha CM, Kim HJ et al (2021) C9orf72-associated arginine-rich dipeptide repeats induce RNA-dependent nuclear accumulation of Staufen in neurons. *Hum Mol Genet* 30:1084–1100. <https://doi.org/10.1093/hmg/ddab089>
  45. Kotian V, Sarmah D, Kaur H, Kesharwani R, Verma G, Mounica L, Veeresh P, Kalia K, Borah A, Wang X et al (2019) Evolving evidence of calcitriol as a pharmacological target in neurological disorders. *ACS Chem Neurosci* 10:2629–2646. <https://doi.org/10.1021/acscchemneuro.9b00158>
  46. Kwon I, Xiang S, Kato M, Wu L, Theodoropoulos P, Wang T, Kim J, Yun J, Xie Y, McKnight SL (2014) Poly-dipeptides encoded by the C9orf72 repeats bind nucleoli, impede RNA biogenesis, and kill cells. *Science* 345:1139–1145. <https://doi.org/10.1126/science.1254917>
  47. LaClair KD, Zhou Q, Michaelsen M, Wefers B, Brill MS, Janjic A, Rathkolb B, Farny D, Cygan M, de Angelis MH et al (2020) Congenic expression of poly-GA but not poly-PR in mice triggers selective neuron loss and interferon responses found in C9orf72 ALS. *Acta Neuropathol* 140:121–142. <https://doi.org/10.1007/s00401-020-02176-0>
  48. Lai JD, Ichida JK (2019) C9ORF72 protein function and immune dysregulation in amyotrophic lateral sclerosis. *Neurosci Lett* 713:134523. <https://doi.org/10.1016/j.neulet.2019.134523>
  49. Lee KH, Zhang P, Kim HJ, Mitrea DM, Sarkar M, Freibaum BD, Cika J, Coughlin M, Messing J, Mollieux A et al (2016) C9orf72 dipeptide repeats impair the assembly, dynamics, and function of membrane-less organelles. *Cell* 167(774–788):e717. <https://doi.org/10.1016/j.cell.2016.10.002>
  50. Lehmer C, Oeckl P, Weishaupt JH, Volk AE, Diehl-Schmid J, Schroeter ML, Lauer M, Kornhuber J, Levin J, Fassbender K et al (2017) Poly-GP in cerebrospinal fluid links C9orf72-associated dipeptide repeat expression to the asymptomatic phase of ALS/FTD. *EMBO Mol Med* 9:859–868. <https://doi.org/10.15252/emmm.201607486>
  51. Leroy E, Boyer R, Auburger G, Leube B, Ulm G, Mezey E, Harta G, Brownstein MJ, Jonnalagada S, Chernova T et al (1998) The ubiquitin pathway in Parkinson's disease. *Nature* 395:451–452. <https://doi.org/10.1038/26652>
  52. Li YR, King OD, Shorter J, Gitler AD (2013) Stress granules as crucibles of ALS pathogenesis. *J Cell Biol* 201:361–372. <https://doi.org/10.1083/jcb.201302044>
  53. Lillo P, Hodges JR (2009) Frontotemporal dementia and motor neurone disease: overlapping clinic-pathological disorders. *J Clin Neurosci* 16:1131–1135. <https://doi.org/10.1016/j.jocn.2009.03.005>
  54. Lin Y, Mori E, Kato M, Xiang S, Wu L, Kwon I, McKnight SL (2016) Toxic PR poly-dipeptides encoded by the C9orf72 repeat expansion target LC domain polymers. *Cell* 167(789–802):e712. <https://doi.org/10.1016/j.cell.2016.10.003>
  55. Liu TY, Yuo CY, Kao CH, Tseng CN, Jong YJ, Chang JG, Wu SM, Chang YF (2011) Hydrogen peroxide decreases the survival rate of HeLa cells with stable knockdown of survival motor neuron protein. *Kaohsiung J Med Sci* 27:102–107. <https://doi.org/10.1016/j.kjms.2010.11.002>
  56. Lopez-Gonzalez R, Lu Y, Gendron TF, Karydas A, Tran H, Yang D, Petrucelli L, Miller BL, Almeida S, Gao FB (2016) Poly(GR) in C9ORF72-related ALS/FTD compromises mitochondrial function and increases oxidative stress and DNA damage in iPSC-derived motor neurons. *Neuron* 92:383–391. <https://doi.org/10.1016/j.neuron.2016.09.015>
  57. Mackenzie IR, Neumann M (2016) Molecular neuropathology of frontotemporal dementia: insights into disease mechanisms from post-mortem studies. *J Neurochem* 138(Suppl 1):54–70. <https://doi.org/10.1111/jnc.13588>
  58. Mann DM, Rollinson S, Robinson A, Bennion Callister J, Thompson JC, Snowden JS, Gendron T, Petrucelli L, Masuda-Suzukake M, Hasegawa M et al (2013) Dipeptide repeat proteins are present in the p62 positive inclusions in patients with frontotemporal lobar degeneration and motor neurone disease associated with expansions in C9ORF72. *Acta Neuropathol Commun* 1:68. <https://doi.org/10.1186/2051-5960-1-68>
  59. Marmor-Kollet H, Siany A, Kedersha N, Knafo N, Rivkin N, Danino YM, Moens TG, Olender T, Sheban D, Cohen N et al (2020) Spatiotemporal proteomic analysis of stress granule disassembly using APEX reveals regulation by SUMOylation and links to ALS pathogenesis. *Mol Cell* 80(876–891):e876. <https://doi.org/10.1016/j.molcel.2020.10.032>
  60. May S, Hornburg D, Schludi MH, Arzberger T, Rentzsch K, Schwenk BM, Grasser FA, Mori K, Kremmer E, Banzhaf-Strathmann J et al (2014) C9orf72 FTLD/ALS-associated Gly-Ala dipeptide repeat proteins cause neuronal toxicity and Unc119 sequestration. *Acta Neuropathol* 128:485–503. <https://doi.org/10.1007/s00401-014-1329-4>
  61. McEachin ZT, Gendron TF, Raj N, Garcia-Murias M, Banerjee A, Purcell RH, Ward PJ, Todd TW, Merritt-Garza ME, Jansen-West K et al (2020) Chimeric peptide species contribute to divergent dipeptide repeat pathology in c9ALS/FTD and SCA36. *Neuron*. <https://doi.org/10.1016/j.neuron.2020.04.011>
  62. McEachin ZT, Parameswaran J, Raj N, Bassell GJ, Jiang J (2020) RNA-mediated toxicity in C9orf72 ALS and FTD. *Neurobiol Dis* 145:105055. <https://doi.org/10.1016/j.nbd.2020.105055>
  63. Meier F, Brunner AD, Frank M, Ha A, Bludau I, Voytk E, Kaspar-Schoenefeld S, Lubeck M, Raether O, Bache N et al (2020) diaPASEF: parallel accumulation-serial fragmentation combined with data-independent acquisition. *Nat Methods* 17:1229–1236. <https://doi.org/10.1038/s41592-020-00998-0>
  64. Moens TG, Niccoli T, Wilson KM, Atilano ML, Birsá N, Gittings LM, Holbling BV, Dyson MC, Thoeng A, Neeves J et al (2019) C9orf72 arginine-rich dipeptide proteins interact with ribosomal proteins in vivo to induce a toxic translational arrest that is rescued by eIF1A. *Acta Neuropathol* 137:487–500. <https://doi.org/10.1007/s00401-018-1946-4>
  65. Mordes DA, Prudencio M, Goodman LD, Klim JR, Moccia R, Limone F, Pietilainen O, Chowdhary K, Dickson DW, Rademakers R et al (2018) Dipeptide repeat proteins activate a heat shock response found in C9ORF72-ALS/FTLD patients. *Acta Neuropathol Commun* 6:55. <https://doi.org/10.1186/s40478-018-0555-8>
  66. Mori K, Arzberger T, Grasser FA, Gijssels I, May S, Rentzsch K, Weng SM, Schludi MH, van der Zee J, Cruts M et al (2013) Bidirectional transcripts of the expanded C9orf72 hexanucleotide repeat are translated into aggregating dipeptide repeat proteins. *Acta Neuropathol* 126:881–893. <https://doi.org/10.1007/s00401-013-1189-3>
  67. Mori K, Weng SM, Arzberger T, May S, Rentzsch K, Kremmer E, Schmid B, Kretzschmar HA, Cruts M, Van Broeckhoven C et al (2013) The C9orf72 GGGGCC repeat is translated into aggregating dipeptide-repeat proteins in FTLD/ALS. *Science* 339:1335–1338. <https://doi.org/10.1126/science.1232927>
  68. Mukkavalli S, Klickstein JA, Ortiz B, Juo P, Raman M (2021) The p97-UBXN1 complex regulates aggresome formation. *J Cell Sci*. <https://doi.org/10.1242/jcs.254201>
  69. Neumann M, Bentmann E, Dormann D, Jawaid A, DeJesus-Hernandez M, Ansorge O, Roerber S, Kretzschmar HA, Munoz DG, Kusaka H et al (2011) FET proteins TAF15 and EWS are selective markers that distinguish FTLD with FUS pathology from amyotrophic lateral sclerosis with FUS mutations. *Brain* 134:2595–2609. <https://doi.org/10.1093/brain/awr201>
  70. Neumann M, Sampathu DM, Kwong LK, Truax AC, Micsenyi MC, Chou TT, Bruce J, Schuck T, Grossman M, Clark CM et al (2006) Ubiquitinated TDP-43 in frontotemporal lobar degeneration and amyotrophic lateral sclerosis. *Science* 314:130–133. <https://doi.org/10.1126/science.1134108>
  71. Nguyen L, Montrasio F, Pattamatta A, Tusi SK, Bardhi O, Meyer KD, Hayes L, Nakamura K, Banez-Coronel M, Coyne A et al (2020) Antibody therapy targeting RAN proteins rescues C9 ALS/FTD phenotypes in C9orf72

- mouse model. *Neuron* 105(645–662):e611. <https://doi.org/10.1016/j.neuron.2019.11.007>
72. Nihei Y, Mori K, Werner G, Arzberger T, Zhou Q, Khosravi B, Japtok J, Hermann A, Sommacal A, Weber M et al (2020) Poly-glycine-alanine exacerbates C9orf72 repeat expansion-mediated DNA damage via sequestration of phosphorylated ATM and loss of nuclear hnRNP A3. *Acta Neuropathol* 139:99–118. <https://doi.org/10.1007/s00401-019-02082-0>
  73. Nonaka T, Masuda-Suzukake M, Hosokawa M, Shimozaawa A, Hirai S, Okado H, Hasegawa M (2018) C9ORF72 dipeptide repeat poly-GA inclusions promote intracellular aggregation of phosphorylated TDP-43. *Hum Mol Genet* 27:2658–2670. <https://doi.org/10.1093/hmg/ddy174>
  74. Ohki Y, Wenninger-Weinzierl A, Hruscha A, Asakawa K, Kawakami K, Haass C, Edbauer D, Schmid B (2017) Glycine-alanine dipeptide repeat protein contributes to toxicity in a zebrafish model of C9orf72 associated neurodegeneration. *Mol Neurodegener* 12:6. <https://doi.org/10.1186/s13024-016-0146-8>
  75. Papadopoulos C, Kirchner P, Bug M, Grum D, Koever L, Schulze N, Poehler R, Dressler A, Fengler S, Arhzaouy K et al (2017) VCP/p97 cooperates with YOD1, UBXD1 and PLAA to drive clearance of ruptured lysosomes by autophagy. *EMBO J* 36:135–150. <https://doi.org/10.15252/embj.201695148>
  76. Raudvere U, Kolberg L, Kuzmin I, Arak T, Adler P, Peterson H, Vilo J (2019) g:Profiler: a web server for functional enrichment analysis and conversions of gene lists (2019 update). *Nucleic Acids Res* 47:W191–W198. <https://doi.org/10.1093/nar/gkz369>
  77. Renton AE, Majounie E, Waite A, Simon-Sanchez J, Rollinson S, Gibbs JR, Schymick JC, Laaksovirta H, van Swieten JC, Myllykangas L et al (2011) A hexanucleotide repeat expansion in C9ORF72 is the cause of chromosome 9p21-linked ALS-FTD. *Neuron* 72:257–268. <https://doi.org/10.1016/j.neuron.2011.09.010>
  78. Riemsdijk FW, Lans H, Seelaar H, Severijnen L, Melhem S, Vermeulen W, Aronica E, Pasterkamp RJ, van Swieten JC, Willemsen R (2019) HR23B pathology preferentially co-localizes with p62, pTDP-43 and poly-GA in C9ORF72-linked frontotemporal dementia and amyotrophic lateral sclerosis. *Acta Neuropathol Commun* 7:39. <https://doi.org/10.1186/s40478-019-0694-6>
  79. Rodriguez-Gonzalez C, Lin S, Arkan S, Hansen C (2020) Co-chaperones DNAJA1 and DNAJB6 are critical for regulation of polyglutamine aggregation. *Sci Rep* 10:8130. <https://doi.org/10.1038/s41598-020-65046-5>
  80. Roux KJ, Kim DI, Raida M, Burke B (2012) A promiscuous biotin ligase fusion protein identifies proximal and interacting proteins in mammalian cells. *J Cell Biol* 196:801–810. <https://doi.org/10.1083/jcb.201112098>
  81. Ruggieri A, Saredi S, Zanotti S, Pasanisi MB, Maggi L, Mora M (2016) DNAJB6 myopathies: focused review on an emerging and expanding group of myopathies. *Front Mol Biosci* 3:63. <https://doi.org/10.3389/fmolb.2016.00063>
  82. Samavarchi-Tehrani P, Samson R, Gingras AC (2020) Proximity dependent biotinylation: key enzymes and adaptation to proteomics approaches. *Mol Cell Proteom* 19:757–773. <https://doi.org/10.1074/mcp.R120.001941>
  83. Sarparanta J, Jonson PH, Kawan S, Udd B (2020) Neuromuscular diseases due to chaperone mutations: a review and some new results. *Int J Mol Sci*. <https://doi.org/10.3390/ijms21041409>
  84. Schludi MH, Becker L, Garrett L, Gendron TF, Zhou Q, Schreiber F, Popper B, Dimou L, Strom TM, Winkelmann J et al (2017) Spinal poly-GA inclusions in a C9orf72 mouse model trigger motor deficits and inflammation without neuron loss. *Acta Neuropathol* 134:241–254. <https://doi.org/10.1007/s00401-017-1711-0>
  85. Schludi MH, May S, Grasser FA, Rentzsch K, Kremmer E, Kupper C, Klopstock T, German Consortium for Frontotemporal Lobar Degeneration, Bavarian Brain Banking Alliance, Arzberger T et al (2015) Distribution of dipeptide repeat proteins in cellular models and C9orf72 mutation cases suggests link to transcriptional silencing. *Acta Neuropathol* 130:537–555. <https://doi.org/10.1007/s00401-015-1450-z>
  86. Schmitz A, Pinheiro Marques J, Oertig I, Maharjan N, Saxena S (2021) Emerging perspectives on dipeptide repeat proteins in C9ORF72 ALS/FTD. *Front Cell Neurosci* 15:637548. <https://doi.org/10.3389/fncel.2021.637548>
  87. Shannon P, Markiel A, Ozier O, Baliga NS, Wang JT, Ramage D, Amin N, Schwikowski B, Ideker T (2003) Cytoscape: a software environment for integrated models of biomolecular interaction networks. *Genome Res* 13:2498–2504
  88. Shorter J (2017) Designer protein disaggregases to counter neurodegenerative disease. *Curr Opin Genet Dev* 44:1–8. <https://doi.org/10.1016/j.gde.2017.01.008>
  89. Sturmer E, Behl C (2017) The role of the multifunctional BAG3 protein in cellular protein quality control and in disease. *Front Mol Neurosci* 10:177. <https://doi.org/10.3389/fnmol.2017.00177>
  90. Szklarczyk D, Franceschini A, Wyder S, Forslund K, Heller D, Huerta-Cepas J, Simonovic M, Roth A, Santos A, Tsafou KP et al (2015) STRING v10: protein–protein interaction networks, integrated over the tree of life. *Nucleic Acids Res* 43:D447–452. <https://doi.org/10.1093/nar/gku1003>
  91. Talbot K, Ansorge O (2006) Recent advances in the genetics of amyotrophic lateral sclerosis and frontotemporal dementia: common pathways in neurodegenerative disease. *Hum Mol Genet* 15(Spec No 2):R182–R187. <https://doi.org/10.1093/hmg/ddl202>
  92. Tang Y, Horikoshi M, Li WX (2016) ggfortify: unified interface to visualize statistical results of popular R packages. *R J* 8:474–485. <https://doi.org/10.32614/rj-2016-060>
  93. Vatsavayai SC, Yoon SJ, Gardner RC, Gendron TF, Vargas JN, Trujillo A, Pribadi M, Phillips JJ, Gaus SE, Hixson JD et al (2016) Timing and significance of pathological features in C9orf72 expansion-associated frontotemporal dementia. *Brain* 139:3202–3216. <https://doi.org/10.1093/brain/aww250>
  94. White MR, Mitrea DM, Zhang P, Stanley CB, Cassidy DE, Nourse A, Phillips AH, Tolbert M, Taylor JP, Kriwacki RW (2019) C9orf72 Poly(PR) dipeptide repeats disturb biomolecular phase separation and disrupt nucleolar function. *Mol Cell* 74(713–728):e716. <https://doi.org/10.1016/j.molcel.2019.03.019>
  95. Wickham H (2016) ggplot2: elegant graphics for data analysis. Springer-Verlag, New York City
  96. Yamakawa M, Ito D, Honda T, Kubo K, Noda M, Nakajima K, Suzuki N (2015) Characterization of the dipeptide repeat protein in the molecular pathogenesis of c9FTD/ALS. *Hum Mol Genet* 24:1630–1645. <https://doi.org/10.1093/hmg/ddu576>
  97. Ye Y, Tang WK, Zhang T, Xia D (2017) A mighty, “protein extractor” of the cell: structure and function of the p97/CDC48 ATPase. *Front Mol Biosci* 4:39. <https://doi.org/10.3389/fmolb.2017.00039>
  98. Yin S, Lopez-Gonzalez R, Kunz RC, Gangopadhyay J, Borufka C, Gygi SP, Gao FB, Reed R (2017) Evidence that C9ORF72 dipeptide repeat proteins associate with U2 snRNP to cause mis-splicing in ALS/FTD patients. *Cell Rep* 19:2244–2256. <https://doi.org/10.1016/j.celrep.2017.05.056>
  99. Zarouchlioti C, Parfitt DA, Li W, Gittings LM, Cheetham ME (2018) DNAJ Proteins in neurodegeneration: essential and protective factors. *Philos Trans R Soc Lond B Biol Sci*. <https://doi.org/10.1098/rstb.2016.0534>
  100. Zhang K, Wang A, Zhong K, Qi S, Wei C, Shu X, Tu WY, Xu W, Xia C, Xiao Y et al (2021) UBQLN2-HSP70 axis reduces poly-Gly-Ala aggregates and alleviates behavioral defects in the C9ORF72 animal model. *Neuron* 109(1949–1962):e1946. <https://doi.org/10.1016/j.neuron.2021.04.023>
  101. Zhang YJ, Gendron TF, Grima JC, Sasaguri H, Jansen-West K, Xu YF, Katzman RB, Gass J, Murray ME, Shinohara M et al (2016) C9ORF72 poly(GA) aggregates sequester and impair HR23 and nucleocytoplasmic transport proteins. *Nat Neurosci* 19:668–677. <https://doi.org/10.1038/nn.4272>
  102. Zhang YJ, Jansen-West K, Xu YF, Gendron TF, Bieniek KF, Lin WL, Sasaguri H, Caulfield T, Hubbard J, Daugherty L et al (2014) Aggregation-prone c9FTD/ALS poly(GA) RAN-translated proteins cause neurotoxicity by inducing ER stress. *Acta Neuropathol* 128:505–524. <https://doi.org/10.1007/s00401-014-1336-5>
  103. Zhou Q, Mareljic N, Michaelsen M, Parhizkar S, Heindl S, Nuscher B, Farny D, Czuppa M, Schludi C, Graf A et al (2020) Active poly-GA vaccination prevents microglia activation and motor deficits in a C9orf72 mouse model. *EMBO Mol Med* 12:e10919. <https://doi.org/10.15252/emmm.201910919>
  104. Zhu Q, Jiang J, Gendron TF, McAlonis-Downes M, Jiang L, Taylor A, Diaz Garcia S, Ghosh Dastidar S, Rodriguez MJ, King P et al (2020) Reduced C9ORF72 function exacerbates gain of toxicity from ALS/FTD-causing repeat expansion in C9orf72. *Nat Neurosci* 23:615–624. <https://doi.org/10.1038/s41593-020-0619-5>

105. Zientara-Rytter K, Subramani S (2019) The roles of ubiquitin-binding protein shuttles in the degradative fate of ubiquitinated proteins in the ubiquitin-proteasome system and autophagy. *Cells*. <https://doi.org/10.3390/cells8010040>
106. Zu T, Liu Y, Banez-Coronel M, Reid T, Pletnikova O, Lewis J, Miller TM, Harms MB, Falchook AE, Subramony SH et al (2013) RAN proteins and RNA foci from antisense transcripts in C9ORF72 ALS and frontotemporal dementia. *Proc Natl Acad Sci USA* 110:E4968-4977. <https://doi.org/10.1073/pnas.1315438110>

### Publisher's Note

Springer Nature remains neutral with regard to jurisdictional claims in published maps and institutional affiliations.

**Ready to submit your research? Choose BMC and benefit from:**

- fast, convenient online submission
- thorough peer review by experienced researchers in your field
- rapid publication on acceptance
- support for research data, including large and complex data types
- gold Open Access which fosters wider collaboration and increased citations
- maximum visibility for your research: over 100M website views per year

**At BMC, research is always in progress.**

Learn more [biomedcentral.com/submissions](https://biomedcentral.com/submissions)

